Application of the semimicroscopic algebraic cluster model to core+α nuclei in the p and sd shells

H. Yépez-Martínez,[1] M. J. Ermamatov,[2,3] P. R. Fraser,[4,5] and P. O. Hess[2]

[1]*Universidad Autónoma de la Ciudad de México, Prolongación San Isidro 151, Col. San Lorenzo Tezonco, Del. Iztapalapa, 09790 México D. F., Mexico*

[2]*Instituto de Ciencias Nucleares, UNAM, Circuito Exterior, C. U., A. P. 70-543, 04510 México, D. F., Mexico*

[3]*Institute of Nuclear Physics, Ulughbek, Tashkent 100214, Uzbekistan*

[4]*Instituto Nazionale di Fisica Nucleare, Sezione di Padova, I-35131, Italy*

[5]*School of Physics, University of Melbourne, Victoria 3010, Australia*

(Received 1 May 2012; revised manuscript received 3 July 2012; published 7 September 2012)

The *semimicroscopic algebraic cluster model* (SACM) is applied to the systems $^{12}C + \alpha \rightarrow {}^{16}O$, $^{14}C + \alpha \rightarrow {}^{18}O$, $^{16}O + \alpha \rightarrow {}^{20}Ne$, $^{18}C + \alpha \rightarrow {}^{22}Ne$, and $^{20}Ne + \alpha \rightarrow {}^{24}Mg$. The spectrum and some $E2$ values are fitted to experiment. Further $E2$ transition values as well as $E1$ and $M1$ transitions are calculated and compared to experiment. In addition, we list the spectroscopic factors of the states listed. These factors are predictions of the model and are of interest in current astrophysical studies.

DOI: 10.1103/PhysRevC.86.034309 PACS number(s): 21.60.Fw, 21.60.Gx, 26.20.Fj, 27.20.+n

I. INTRODUCTION

The semimicroscopic algebraic cluster model (SACM) is a model for nuclear cluster structure which incorporates the Pauli exclusion principle, which is, in general, difficult to implement microscopically for complex systems, because the large dimensions of the resulting space lead to large computational difficulties. However, incorporating the Pauli principle in a semimicroscopic model is of greater ease.

It has been applied with success to several light nuclear systems [1,2]. However, until now, applications have mainly regarded the study of the energy spectra and $E1$, $E2$, and $M1$ electromagnetic transitions of nuclei considered to be described by a single dynamical symmetry [1–4]. Recently though, some applications have been published that allow nuclei to be described by a mixing of dynamical symmetries [5,6]. The aim of this contribution is to present an algebraic model which is able to describe not only the energy spectra and electromagnetic transitions of nuclei but also spectroscopic factors, and all in cases of the breaking of dynamical symmetries.

In the SACM [1,2], the internal structure of the clusters is described by the shell model, having a $U^{ST}(4) \otimes U(3)$ group structure, where $U^{ST}(4)$ stands for the spin-isospin sector, while $U(3)$ refers to the space-part. The model for a binary clusterization then has a $U_{C_1}^{ST}(4) \otimes U_{C_1}(3) \otimes U_R(4) \otimes U_{C_2}^{ST}(4) \otimes U_{C_2}(3)$ algebraic structure, where C_i stands for the ith cluster and R indicates relative motion. The model space is constructed to be free from Pauli-forbidden states, and the physical operators are expressed in terms of the group-generators. If we consider spin-isospin zero clusters, which is going to be the case here, then the role of the $U_{C_i}^{ST}(4)$ groups is important only in the construction of the model space, and they do not play any role in formulating physical operators. Therefore, from the viewpoint of the interactions, the group structure is simplified to $U_{C_1}(3) \otimes U_R(4) \otimes U_{C_2}(3)$. (This model has been applied in realistic studies [3,4].)

The interactions considered in the Hamiltonian of the present model can be expressed in terms of the algebraic operators, up to second order, in terms of the group generators. Some exceptional interactions of third order are added, the first being a correction to the quadrupole-quadrupole interaction, and the second being the Casimir-invariant of third order $\boldsymbol{C}_3(\mathrm{SU}(3))$, of the largest coupled group $U_{C_1}(3) \otimes U_R(4) \otimes U_{C_2}(3)$. This last type of interaction has been considered in order to shift the (λ, μ) of the total SU(3) irreducible representation (irrep), from the (μ, λ) irrep. The Hamiltonian considered here is similar to other algebraic Hamiltonians for the study of nuclear clusterization [7], with the addition of an SO(4)-type interaction that breaks the dynamical symmetry of the SACM model.

Its parameters are fit to the energy spectra of the nuclei and some $E2$ transitions. While the $B(E2)$ transitions are adjusted in the fit, the $B(E1)$ and $B(M1)$ transitions and the spectroscopic factors are predictions of the model. The effective charges are determined via a geometrical mapping, while for the $B(E2)$ values a further correction factor is introduced, which measures the deviation from the geometrical estimate [8].

This model is applied to the core+α nuclei $^{12}C + \alpha \rightarrow {}^{16}O$, $^{14}C + \alpha \rightarrow {}^{18}O$, $^{16}O + \alpha \rightarrow {}^{20}Ne$, $^{18}O + \alpha \rightarrow {}^{22}Ne$, and $^{20}Ne + \alpha \rightarrow {}^{24}Mg$. These systems play a very important role in astrophysics in order to produce heavier elements, defined as the *secondary α fusion process*, which occurs in stars when some carbon is initially present. The reaction corresponding to the first system has a Q value of 7.16 MeV. The third, fourth, and fifth systems have Q values of 4.73, 9.31, and 6.95 MeV, respectively. These are the dominant reactions and the knowledge of spectroscopic factors is needed.

The first system examined is of great importance. The radiative capture reaction $^{12}C(\alpha, \gamma)^{16}O$ is widely considered to be among the most important processes in stellar nucleogenesis—it is Hoyle's "holy grail." It determines the mass ratio of ^{12}C and ^{16}O after helium burning, and, thus, the abundances of elements from carbon to iron and, in turn, the iron-core mass at supernova explosion, for massive stars [9,10].

For stellar models to be useful, the total scattering cross section for this reaction must be known, to within 20%

accuracy, in the Gamow window around $E_{\text{c.o.m.}} = 0.3$ MeV. This is not currently feasible experimentally, and, indeed, the lowest energy of any scattering experiment performed for this system was $E_{\text{c.o.m.}} = 0.75$ MeV [11].

Thus, theoretical investigations of scattering in the important energy regime are needed. The most recent [12] sought a simple expression for asymptotic normalization constants based on a very old model-independent prescription of the S matrix [13], and results of this expression were tested against numerical results, using an even older potential [14,15]. Another recent paper [16] sought cross sections using optical potentials, another very old approach. While important works that showed good results, these indicate that more modern, sophisticated theoretical approaches, showing greater insight into nuclear structure, are needed. (For a brief overview of work to date on this reaction, see Ref. [17].)

While the present work is not concerned with scattering, works that contribute $\alpha + {}^{12}$C potentials, from a structural point of view, are useful in that they may be used in scattering formalisms to extract elastic [18] and radiative capture [19] cross sections.

The structure of this paper is as follows. In Sec. II, details of the SACM are presented, including itstwo-cluster Hamiltonian. Section III details the electromagnetic transition operators, as well as their geometric mapping, providing one general method for obtaining the effective charges. In Sec. IV the parametrization of the spectroscopic factor is presented. Section V presents numerical applications of the model. Finally, in Sec. VI some conclusions are drawn. For completeness, and also as such is nowhere else available, the appendices list the formulas for all possible interaction terms and transition operators.

II. THE MODEL

A. The semimicroscopic algebraic cluster model space

In the SACM the internal structure of the clusters are described by the Elliott shell model with a $U_{C_i}^{ST}(4) \otimes U_{C_i}(3)$ group structure. Their internal wave functions are completely antisymmetric. However, when the product wave function of the two clusters and that of the relative motion is constructed, it is contaminated by Pauli-forbidden states, as antisymmetrization with respect to the interchange of nucleons between the two clusters is not taken into account. Therefore, the Pauli principle must be incorporated by some supplementary means. There are several ways to do this, and for the light binary-cluster configurations considered here, a suitable and simple procedure is to take the intersection of the non-anti-symmetric cluster-model basis and the fully antisymmetric-shell-model basis of the united nucleus. Such is done here, with details discussed in Ref. [2]. When this procedure is applied to a system of two closed-shell clusters, it reduces to the Wildermuth condition, which simply gives a lower limit for the number of quanta of the relative motion [20] (which, of course, depends on the specific clusters). When one or both clusters have an open shell, a more refined discrimination between allowed and forbidden single-nucleon states within a major shell is required. Thus, when constructing the microscopic model space, the spin-isospin degrees of freedom [the $U^{ST}(4)$ group] play an essential role; without them, the consequences of the antisymmetrization cannot be taken into account. For more details, please consult Refs. [1,2,21,22].

B. The Hamiltonian

If restricted to a single sector of the spin-isospin degrees of freedom when constructing the Hamiltonian, as is the case in what follows, the basis of the SACM can be characterized by the following group structure:

$$\begin{array}{ccccc} \mathrm{SU}_{C_1}(3) \otimes \mathrm{SU}_{C_2}(3) \otimes \mathrm{SU}_R(3) & \supset & \mathrm{SU}_C(3) \otimes \mathrm{SU}_R(3) & \supset & \\ (\lambda_1,\mu_1)(\lambda_2,\mu_2) & & (n_\pi,0) & & (\lambda_C,\mu_C) \\ \mathrm{SU}(3) & \supset & \mathrm{SO}(3) & \supset & \mathrm{SO}(2) \\ (\lambda,\mu) & & \kappa L & & M, \end{array} \tag{1}$$

where (λ_k, μ_k) refer to the $\mathrm{SU}_{C_k}(3)$ irreducible representations (irreps) of the individual clusters, which are coupled to intermediate irrep (λ_C, μ_C), n_π is the number of relative oscillator quanta, while (λ, μ) is the total SU(3) irrep. L and M are the angular momentum and its projection, and κ is the eigenvalue of the $\boldsymbol{K}^2$ operator [1,2,23], which classifies the rotational bands, giving the projection of the angular momentum onto the intrinsic z axis, distinguishing multiple occurrences of a given L in (λ, μ).

Beginning with the Hamiltonian of Refs. [21,22], we add further terms which allow reproduction of the order of negative-parity states, which in ^{16}O is 3^-, 1^-, and 2^-. Namely

$$\boldsymbol{H} = xy\boldsymbol{H}_{\mathrm{SU}(3)} + y(1-x)\boldsymbol{H}_{\mathrm{SO}(4)} + (1-y)\boldsymbol{H}_{\mathrm{SO}(3)}, \tag{2}$$

with x and y being mixing parameters of the dynamical symmetries with values between 0 and 1, and

$$\begin{aligned} \boldsymbol{H}_{\mathrm{SU}(3)} &= \hbar\omega\boldsymbol{n}_\pi + a_{\mathrm{Clus}}C_2(\lambda_C,\mu_C) + (a - b\Delta\boldsymbol{n}_\pi)C_2(\lambda,\mu) \\ &\quad + (\bar{a} - \bar{b}\Delta\boldsymbol{n}_\pi)C_2(\boldsymbol{n}_\pi,0) + t_1C_3(\lambda,\mu) \\ &\quad + (\gamma + a_L(-1)^L + a_{Ln}\Delta\boldsymbol{n}_\pi)\boldsymbol{L}^2 + t\boldsymbol{K}^2 \\ \boldsymbol{H}_{\mathrm{SO}(4)} &= a_C{\boldsymbol{L}_C}^2 + a_R^{(1)}{\boldsymbol{L}_R}^2 + (\gamma + a_L(-1)^L)\boldsymbol{L}^2 \\ &\quad + \frac{c}{4}[(\boldsymbol{\pi}^\dagger\cdot\boldsymbol{\pi}^\dagger) - (\sigma^\dagger)^2][(\boldsymbol{\pi}\cdot\boldsymbol{\pi}) - (\sigma)^2] \\ \boldsymbol{H}_{\mathrm{SO}(3)} &= \hbar\omega\boldsymbol{n}_\pi + a_{\mathrm{Clus}}C_2(\lambda_C,\mu_C) + a_C{\boldsymbol{L}_C}^2 + a_R^{(1)}\boldsymbol{L}_R^2 \\ &\quad + (\gamma + a_L(-1)^L + a_{Ln}\Delta\boldsymbol{n}_\pi)\boldsymbol{L}^2, \end{aligned} \tag{3}$$

where $\Delta\boldsymbol{n}_\pi = \boldsymbol{n}_\pi - n_0$, n_0 being the minimal number of quanta required by the Pauli principle. The a_{Clus} is the strength of the quadrupole-quadrupole interaction, restricted to the cluster part, while R and C denote the contributions related to the *relative* and *cluster* part, respectively, and $\boldsymbol{L}^2$ is the total angular-momentum operator.

For the case of two spherical clusters, the second-order Casimir operator of SU(3) is $\boldsymbol{n}_\pi(\boldsymbol{n}_\pi + 3)$. Note that in the case of deformed clusters the information about the deformation only enters in the SU(3) dynamical limit.

The difference between Eqs. (2) and (3) and the Hamiltonian used in Refs. [21,22] is in the coefficient of the angular-momentum operator. This coefficient now depends on L and Δn_π, which represents a dependence of the moment of

inertia on the angular momentum and the number of shell excitations. This ansatz is not new, being used before in Refs. [3,4].

The first term of the SU(3) Hamiltonian, $\hbar\omega \boldsymbol{n}_\pi$, contains the linear invariant operator of the $U_R(3)$ subgroup, and $\hbar\omega$ is usually chosen to be $(45A^{-1/3} - 25A^{-2/3})$ for light nuclei [24] and $41A^{-1/3}$ for heavy nuclei [25]. When a truncation is applied due to the exclusion principle, one finds that n_π has a minimal value larger than zero.

The $\boldsymbol{C}_2$ (SU(3)) is the second-order Casimir invariant of the largest coupled SU(3) group of Eq. (1), having contributions both from the internal cluster part and from the relative motion, and is given by

$$\begin{aligned} \boldsymbol{C}_2(\mathrm{SU}(3)) &= \tfrac{1}{4}\boldsymbol{Q}^2 + \tfrac{3}{4}\boldsymbol{L}^2, \\ &\rightarrow (\lambda^2 + \lambda\mu + \mu^2 + 3\lambda + 3\mu), \\ \boldsymbol{Q} &= \boldsymbol{Q}_C + \boldsymbol{Q}_R, \\ \boldsymbol{L} &= \boldsymbol{L}_C + \boldsymbol{L}_R, \end{aligned} \tag{4}$$

where $\boldsymbol{Q}$ and $\boldsymbol{L}$ are the quadrupole operator and angular-momentum operator, respectively. The relations of the quadrupole and angular-momentum operators to the $C^{(1,1)}_{2m}$ generators of the SU(3) group, expressed in terms of SU(3)-coupled π-boson creation and annihilation operators [26], are

$$\begin{aligned} \boldsymbol{Q}_{k\,2m} &= \frac{1}{\sqrt{3}} C^{(1,1)}_{2m}, \quad \boldsymbol{Q}_{R\,2m} = \sqrt{3} C^{(1,1)}_{2m}, \\ \boldsymbol{L}_{1m} &= C^{(1,1)}_{1m}, \quad \boldsymbol{C}^{(1,1)}_{lm} = \sqrt{2}[\boldsymbol{\pi}^\dagger \otimes \boldsymbol{\pi}]^{(1,1)}_{lm}. \end{aligned} \tag{5}$$

Numerical values of these can be found in Refs. [27,28]. The subscripted R, C, and $k = 1, 2$ are used to distinguish the quadrupole operator associated with the relative motion from the quadrupole operator of the clusters or quadrupole operator of the coupled clusters. (The reason for considering two different numerical factors for these quadrupole operators is discussed in more detail in the next section.) The remaining subscripts denote SO(3) and SO(2) quantum numbers, and superscripts denote SU(3).

The matrix elements of all the terms of the Hamiltonian in Eq. (2) and (3) can be calculated by standard SU(3) coupling and recoupling techniques [26]; the relevant formulas are collected in Appendix A for the SO(4)-like interaction and for the different quadrupole and angular-momentum terms.

III. ELECTROMAGNETIC TRANSITIONS AND THE GEOMETRICAL MAPPING

The model detailed in the previous section considers the electromagnetic transition operator, $T^{(\bar{\lambda}_j,\bar{\mu}_j)k_j l_j}_{m_j}$, to also have an $\mathrm{SU}_j(3)$ character, with $j = 1, 2, C$, or R. In the present work only the electric dipole ($E1$), the electric quadrupole ($E2$), and the magnetic dipole ($M1$) transition operators will be discussed,

$$\begin{aligned} \boldsymbol{T}^{(E1)}_m &= e^{(1)}_R \boldsymbol{D}^{(1)}_{R,m}, \quad \boldsymbol{T}^{(E2)}_m = \sum_\gamma e^{(2)}_\gamma \boldsymbol{Q}^{(2)}_{\gamma,m}, \\ \boldsymbol{T}^{(M1)}_m &= \sum_\gamma m^{(1)}_\gamma \boldsymbol{L}^{(1)}_{\gamma,m}, \end{aligned} \tag{6}$$

using the notation of previous works [1,2].

In what follows, the transition operators of Eq. (6) are each discussed separately. The purpose of this part of the model is to obtain a relationship between the effective charges and geometrical variables and, therefore, a means of estimating effective charges. Each total transition operator may be multiplied by a parameter, which can be considered to be a correction to the geometrically estimated effective charge. (In this contribution only the $E2$ transition involves such a correction factor.) The closer this factor is to 1, the better the quality of the geometrical estimate.

To obtain the above-mentioned geometrical relationship for the case of the relative motion, we use a geometrical mapping, in similar form as in Ref. [8]. For the individual clusters and the coupled cluster (C) part, the geometrical connection between effective charges and geometrical variables is also similar to those given in Refs. [8,29].

A. Electromagnetic effective charges

1. Electric quadrupole transition operator

The total $E2$ transition operator is given by

$$\boldsymbol{T}^{(E2)}_m = \left(\frac{5}{16\pi}\right)^{\frac{1}{2}} p_{e2}\left[e^{(2)}_1 \boldsymbol{Q}^{(2)}_{1,m} + e^{(2)}_2 \boldsymbol{Q}^{(2)}_{2,m} + e^{(2)}_R \boldsymbol{Q}^{(2)}_{R,m}\right], \tag{7}$$

where $e^{(2)}_k$ are effective charges of clusters 1 and 2 and $e^{(2)}_R$ is the same for relative motion. Here, the quadrupole transition operator is expressed as the sum of the quadrupole momentum operator, $Q^{(2)}_j$, associated with the different $\mathrm{SU}_j(3)$ group, with $j = 1$, 2, and R. One could include the coupled quadrupole operator $\boldsymbol{Q}^{(2)}_{C,m}$, but this term can be expressed as a sum of $\boldsymbol{Q}^{(2)}_{1,m}$ and $\boldsymbol{Q}^{(2)}_{2,m}$, and with a simple rearrangement of terms Eq. (7) is again obtained. The factor p_{e2} is the aforementioned correction to the geometrical estimate.

Note that the *mass quadrupole operator* is considered here. In order to have the *charge quadrupole operator* one must multiply the mass quadrupole operator of the cluster k by $\frac{Z_k}{A_k}$ and the relative mass quadrupole operator by $\frac{Z}{A}$. Therefore, the final expression for $\boldsymbol{T}^{(E2)}_m$ is

$$\begin{aligned} &\boldsymbol{T}^{(E2)}_m \\ &= \left(\frac{5}{16\pi}\right)^{\frac{1}{2}} \left[e^{(2)}_1 \frac{Z_1}{A_1} \boldsymbol{Q}^{(2)}_{1,m} + e^{(2)}_2 \frac{Z_2}{A_2} \boldsymbol{Q}^{(2)}_{2,m} + e^{(2)}_R \frac{Z}{A} \boldsymbol{Q}^{(2)}_{R,m}\right]. \end{aligned} \tag{8}$$

The individual cluster contribution to the geometrical mapping, which relates the effective charge to the total number of oscillation quanta and the deformation, is [8]

$$\left\langle e^{(2)}_k \boldsymbol{Q}^{(2)}_{k,m} \right\rangle = \sqrt{\frac{5}{\pi}} N_{0,k} \alpha_{2m}(k), \tag{9}$$

where k denotes cluster 1 or 2 and $N_{0,k}$ is the total number of oscillation quanta plus $\frac{3}{2}(A_k - 1)$. The A_k is the total number of nucleons in cluster k.

For simplicity, we consider the $m = 0$ component of the deformation α_{2m}. The $\alpha_{20}(k)$ in the intrinsic system is just

$\beta(k)$, i.e., the deformation parameter of the kth cluster. The expectation of the algebraic quadrupole operator with spin two and projection zero with respect to a SU(3) basis is given by

$$\begin{aligned}\langle(\lambda_k,\mu_k)\kappa_k = 1 L_k = 2 M_k = 0|Q_{20}|(\lambda_k,\mu_k)\kappa_k \\ = 1 L_k = 2 M_k = 0\rangle \\ = \langle(\lambda_k,\mu_k)12,(1,1)12||(\lambda_k,\mu_k)12\rangle_1 \\ \times (20,20|20)2(-1)^{\phi}\sqrt{C_2(\lambda_k,\mu_k)} \\ = Q_0(\lambda_k,\mu_k).\end{aligned} \tag{10}$$

The first factor refers to an isoscalar factor [26], the second factor is a SU(2) Clebsch-Gordan coefficient, $C_2(\lambda,\mu) = (\lambda^2+\lambda\mu+\mu^2+3\lambda+3\mu)$, and ϕ is 1 for $\mu \neq 0$ and 0 for $\mu = 0$. The factor $2(-1)^{\phi}\sqrt{C_2(\lambda_k,\mu_k)}$ is the triply reduced matrix element of the quadrupole operator, which is a generator of $\mathrm{SU}_k(3)$ [26].

Therefore, the geometrical estimate of the effective charge for the quadrupole cluster transition operator is given by

$$e_k^{(2)} = \sqrt{\frac{5}{\pi}} N_{0,k}\beta_{0,k}/Q_0(\lambda_k,\mu_k). \tag{11}$$

Likewise, the effective charge for the radial quadrupole transition operator associated with the relative motion can be evaluated by the geometrical mapping of the algebraic transition operator $\boldsymbol{T}^{(E2)}_{R,m}$, in this case taking the limit $N \to \infty$, as was the case in Ref. [8]. This mapping has to be of the order of

$$\left\langle \boldsymbol{T}^{(E2)}_{R,m}\right\rangle = \frac{Z}{A}\left\langle e_R^{(2)}\boldsymbol{Q}^{(2)}_{R,m}\right\rangle \approx \sqrt{6}\frac{Z}{A}[r\times r]^{[2]}_m \tag{12}$$

(not considering the additional factor p_{e2}). Furthermore, it is necessary to remember that the transition operator of Eq. (12) is an algebraic operator without units. In order to obtain the correct effective charge, one has to multiply by $\frac{\hbar}{m\omega}$, obtaining

$$\left\langle \boldsymbol{T}^{(E2)}_{R,m}\right\rangle = \frac{Z}{A}\frac{\hbar}{m\omega}\left\langle e_R^{(2)}\boldsymbol{Q}^{(2)}_{R,m}\right\rangle \approx \sqrt{6}\frac{Z}{A}[r\times r]^{[2]}_m. \tag{13}$$

It is important to note that in the definition $\langle \boldsymbol{T}^{(E2)}_{R,m}\rangle = \sqrt{6}\frac{Z}{A}[r\times r]^{[2]}_m$, a $\sqrt{6}$ factor has been considered, instead of $\frac{\sqrt{3}}{2}$ as it was used in Refs. [1,2]. The definition used here is closer to that of the physical definition of the quadrupole operators, where the $m=0$ projection has to be given by $2z^2-x^2-y^2$ for the coordinate-dependent term. Now the geometrical mapping of the $\boldsymbol{Q}^{(2)}_{R,m}$ operator (where $\boldsymbol{Q}^{(2)}_{R,m} = \sqrt{6}[\pi^{\dagger}\times\tilde{\pi}]^{[2]}_m$) is given by

$$\left\langle \boldsymbol{Q}^{(2)}_{R,m}\right\rangle \approx \sqrt{6}N[\alpha\times\alpha]^{[2]}_m. \tag{14}$$

Using the results obtained previously in Ref. [8], one obtains

$$\alpha_m \approx \sqrt{\frac{\mu\omega_r}{2N\hbar}}(r_m - r_{0,m}), \tag{15}$$

where μ is the reduced mass and $\omega_r = \sqrt{\frac{A_1+A_2}{A_1A_2}}\omega$ [30]. These factors arise from the consideration that the oscillator constant, $m\omega^2$, changes after a transformation in the radial part to $\mu\omega_r^2$, due to the condition that $m\omega^2 = \mu\omega_r^2$. Using, for simplicity, $r_{0,m}=0$, Eq. (13) can be expressed as (again, not considering the additional factor p_{e2})

$$\left\langle \boldsymbol{T}^{(E2)}_{R,m}\right\rangle = \frac{Z}{A}\frac{\hbar}{m\omega}\left\langle e_R^{(2)}\boldsymbol{Q}^{(2)}_{R,m}\right\rangle = \sqrt{6}e_R^{(2)}\frac{Z}{A}\frac{\mu\omega_r}{2m\omega}[r\times r]^{[2]}_m. \tag{16}$$

This has to be compared to the classical definition of the quadrupole operators. Comparing Eq. (12) and (16), one obtains

$$e_R^{(2)} = 2\frac{m\omega}{\mu\omega_r} = 2\sqrt{\frac{A_1+A_2}{A_1A_2}}. \tag{17}$$

2. Electric dipole transition operator

The expectation value of the $E1$ transition operator is given by [8]

$$\begin{aligned}\left\langle p_{e1}e_R^{(1)}\boldsymbol{D}^{(1)}_{R,m}\right\rangle &= p_{e1}e_R^{(1)}\langle\pi_m^{\dagger}s + s^{\dagger}\pi_m\rangle \\ &\approx 2p_{e1}\left(e_R^{(1)}\sqrt{N}\right)\sqrt{\frac{\mu\omega_r}{2\hbar}}(r_m - r_{0,m}).\end{aligned} \tag{18}$$

Note that this expectation value has no units. In order to compare it with the geometrical dipole operator, one must multiply the above by $\sqrt{\frac{\hbar}{m\omega}}$. The possible additional factor, p_{e1}, again serves to model the deviation from the geometric estimate. In the applications to core+α nuclei in the p and sd shells, however, we will not adjust $E1$ transitions and, instead, using the value $p_{e1}=1$.

The classical definition of the geometrical dipole moment for two charges, Z_1 and Z_2, separated by distance r_0, divided by the unit charge e, and with $m=0$, is given by

$$D_0^{\mathrm{geom}} = \frac{A_1A_2}{A}\left(\frac{Z_1}{A_1} - \frac{Z_2}{A_2}\right)r_0. \tag{19}$$

Compared with Eq. (18), and using, for simplicity, $r_{0,m}=0$, one obtains

$$e_R^{(1)}\sqrt{N} = \frac{A_1A_2}{A}\left|\left(\frac{Z_1}{A_1} - \frac{Z_2}{A_2}\right)\right|\sqrt{\frac{m\omega}{2\mu\omega_r}}, \tag{20}$$

where the modulus was taken because the sign enters in the formula for D_0^{geom}. It is important to note that for the electric dipole operator the effective charge depends on the total number of bosons considered, N, or, in other words, on the "cutoff."

3. Magnetic dipole transition operator

The magnetic dipole transition operator $\boldsymbol{T}^{(M1)}$ is defined as

$$\boldsymbol{T}^{(M1)} = \mu_0\left[g_1\boldsymbol{L}^{(1)}_m + g_2\boldsymbol{L}^{(2)}_m + g_R\boldsymbol{L}_R\right]. \tag{21}$$

No additional factor which would account for the deviation from the geometrical estimate is introduced. The gyromagnetic factors are given by $g_k = \frac{Z_k}{A_k}$ [25], and for the radial motion it is $g_R = \frac{Z}{A}$.

The factors in Eq. (21) also give an expression for the effective charges in front of the magnetic dipole transition

operator considered in Eq. (6), i.e,

$$m_k^{(1)} = \mu_0 \frac{Z_k}{A_k}, \quad m_R^{(1)} = \mu_0 \frac{Z}{A}, \tag{22}$$

with $k = 1$ or 2.

B. Electromagnetic matrix elements

In order to evaluate the electromagnetic transition intensities, we calculate the matrix elements of the transitions operators of Eq. (6) between different total irreps and total spin.

The electromagnetic transition rates will be determined by the reduced matrix element

$$\langle (\lambda_1', \mu_1'), (\lambda_2', \mu_2'); \rho_C'(\lambda_C', \mu_C'), (n_\pi', 0); (\lambda', \mu') K' L' || T^{(\bar{\lambda_j}, \bar{\mu_j}) k_j l_j} || (\lambda_1, \mu_1), (\lambda_2, \mu_2); \rho_C(\lambda_C, \mu_C), (n_\pi, 0); (\lambda, \mu) K L \rangle \tag{23}$$

via the relation (with $\omega = E$ or M, for an electric or magnetic transition, respectively):

$$B(\omega l; L \to L') = \frac{2L'+1}{2L+1} |\langle \alpha' L' || T^{(\bar{\lambda}, \bar{\mu}) k l} || \alpha L \rangle|^2. \tag{24}$$

Note that Eq. (24) reflects the form of the Wigner-Eckart theorem and the definition of the doubly reduced matrix elements followed by Escher and Draayer [26].

The different electromagnetic transitions ($E1$, $E2$, and $M1$) considered here can be evaluated from the matrix elements of Eq. (23) by defining the transition operator with the appropriate tensorial character, and these matrix elements can be calculated by standard SU(3) techniques [26]; the relevant formulas are collected in Appendix B.

In order to obtain the transition intensities between different states, it is important to remember that the $\boldsymbol{Q}^{(2)}_{k,m_j}$ operators and the angular-momentum operator $\boldsymbol{L}^{(1)}_{k,m_j}$ are proportional to the rank-2 generators of the $\mathrm{SU}_j(3)$ groups as given in Eq. (5).

IV. SPECTROSCOPIC FACTORS

Here, we summarize the evaluation of the spectroscopic factors within the model. For a more detailed discussion, please consult Refs. [6,31].

The first attempt to calculate the spectroscopic factors within the SACM was published in Ref. [32] and applied to nuclei in the p and sd shells. Then, in Ref. [31], an exponential ansatz, multiplied by SU(3) isoscalar factors, was proposed as follows:

$$\begin{aligned} S_{\mathrm{SU(3)}} = \exp[&A + Bn_\pi + C\mathcal{C}_2(\lambda_1, \mu_1) + D\mathcal{C}_2(\lambda_2, \mu_2) \\ &+ E\mathcal{C}_2(\lambda_c, \mu_c) + F\mathcal{C}_2(\lambda, \mu) + G\mathcal{C}_3(\lambda, \mu) + H\Delta n_\pi] \\ &\times |\langle (\lambda_1, \mu_1)\kappa_1 L_1, (\lambda_2, \mu_2)\kappa_2 L_2 || (\lambda_C, \mu_C)\kappa_C L_C \rangle_{\rho_C} \\ &\times \langle (\lambda_C, \mu_C)\kappa_C L_C, (n_\pi, 0) 1 l || (\lambda, \mu)\kappa L \rangle_1|^2, \end{aligned} \tag{25}$$

where $\mathcal{C}_3(\lambda, \mu)$ is the third-order Casimir operator of SU(3) with eigenvalue $(\lambda - \mu)(2\lambda + \mu + 3)(\lambda + 2\mu + 3)$, which is important when distinguishing between excited states (λ, μ) and (μ, λ). The $\mathcal{C}_2(\lambda_k, \mu_k)$ $(k = 1, 2, C)$ is the second-order Casimir operator with eigenvalue $(\lambda_k^2 + \lambda_k\mu_k + \mu_k^2 + 3\lambda_k + 3\mu_k)$. Finally, $\Delta n_\pi = (n_\pi - n_o)$ is as in Eq. (3), and l is the angular momentum of the relative motion. This formula is valid only for even-even nuclei, to which we restrict ourselves here.

TABLE I. Parameter values used in the spectroscopic factor.

A	B	C	D
2.1466	−0.361 13	−0.054 389	−0.117 64
E	F	G	H
0.060 728	−0.008 665 4	0.000 021 097	1.909 01

In Ref. [31], the parameters of this equation were fitted to 17 states of core+α systems within the p and sd shells. Because the applications in this contribution are also core+α nuclei, we use the same parameter values, with one exception (outlined below). These values are listed in Table I.

The single divergence between the values used [31] and those used herein is the parameter A; it was chosen in Ref. [31] such that is gives 1 for the ground state of $^{16}\mathrm{O} + \alpha$, and the value given here was chosen in order to reproduce the absolute value of 0.23, as given by the microscopic calculation of Ref. [33].

In Ref. [31], the spectroscopic factors of about 100 further states were calculated, with agreement to within a couple of percentages of the SU(3) microscopic calculations. Mainly, core+α states were considered, though 15 states were included from the $^{12}\mathrm{C} + {}^{12}\mathrm{C}$ and $^{16}\mathrm{O} + {}^{8}\mathrm{Be}$ systems.

The structure of the spectroscopic factor can be understood by the following arguments: The probability of finding two clusters separated by a distance R is proportional to

TABLE II. The values of the parameters determined by fitting calculations to data.

	$^{12}\mathrm{C}+\alpha$	$^{14}\mathrm{C}+\alpha$	$^{16}\mathrm{O}+\alpha$	$^{18}\mathrm{O}+\alpha$	$^{20}\mathrm{Ne}+\alpha$
$\hbar\omega$	13.921	13.531	13.185	12.876	12.595
a	−0.621	−0.0005	−0.469	−0.439	−1.377
$\bar{a}$	−0.230	−0.426	0.000	−0.097	−0.135
γ	0.111	0.184	0.175	0.349	0.211
a_{Clus}	0.000	0.000	0.000	0.000	0.000
b	−0.023	−0.000 04	−0.001	−0.030	0.012
$\bar{b}$	−0.028	−0.027	0.000	−0.007	−0.009
c	−2.232	0.706	0.483	0.200	−0.772
a_C	0.036	0.763	0.000	1.367	0.555
$a_R^{(1)}$	0.163	0.143	0.000	−0.0661	0.403
t	0.000	0.672	0.000	0.784	0.638
t_1	0.000	0.000	0.000	0.000	0.000
a_L	0.163	0.060	0.056	−0.179	−0.010
a_{Ln}	−0.037	−0.018	−0.079	0.87×10^{-3}	−0.220
p_{e2}	1.447	0.334	0.930	0.689	0.346
x	0.943	0.706	0.784	0.950	0.917
y	1.000	1.000	1.000	1.000	1.000

TABLE III. The calculated and experimental values of the energy levels with positive parities.

L	$^{12}C+\alpha$		L	$^{14}C+\alpha$		L	$^{16}O+\alpha$		L	$^{18}O+\alpha$		L	$^{20}Ne+\alpha$	
	Calc.	Expt.		Calc.	Expt.		Calc.	Expt.		Calc.	Expt.		Calc.	Expt.
0_1^+	0.00	0.00	0_1^+	0.00	0.00	0_1^+	0.	0.00	0_1^+	0.00	0.00	0_1^+	0.00	0.00
0_2^+	5.75	6.05	0_2^+	3.65	3.63	0_2^+	8.21	6.73	0_2^+	3.55		0_2^+	4.88	6.43
0_3^+	7.50	11.26	0_3^+	15.16		0_3^+	14.60	7.19	0_3^+	5.41		0_3^+	9.85	10.68
0_4^+	12.07	12.05	0_4^+	17.94		0_4^+	20.29	11.56	0_4^+	12.14		0_4^+	15.25	11.72
0_5^+	16.60	14.03	0_5^+	31.20		0_5^+	25.62	12.43	0_5^+	16.03		0_5^+	19.42	13.04
1_1^+	12.48	17.14	1_1^+	24.12		2_1^+	1.57	1.63	1_1^+	4.13	5.33	1_1^+	17.13	7.75
1_2^+	15.02		1_2^+	41.21		2_2^+	9.06	7.42	1_2^+	10.90	6.86	1_2^+	21.27	9.83
1_3^+	22.73		1_3^+	59.86		2_3^+	14.85	7.83	1_3^+	16.40		1_3^+	24.65	9.97
1_4^+	28.47		1_4^+	82.38		2_4^+	19.96	9.49	1_4^+	26.11		1_4^+	47.55	10.71
1_5^+	33.49		1_5^+			2_5^+	24.67	10.27	1_5^+	31.51		1_5^+	61.06	
2_1^+	7.17	6.92	2_1^+	1.23	1.98	4_1^+	5.14	4.25	2_1^+	1.04	1.28	2_1^+	1.41	1.37
2_2^+	8.42	9.85	2_2^+	4.12	3.92	4_2^+	10.88	9.03	2_2^+	4.00	4.46	2_2^+	3.45	4.24
2_3^+	13.04	11.52	2_3^+	5.14	5.25	4_3^+	15.35	9.99	2_3^+	4.20	6.34	2_3^+	6.48	7.35
2_4^+	14.53	13.02	2_4^+	16.14	8.21	4_4^+	19.19	11.09	2_4^+	4.68		2_4^+	9.90	8.65
2_5^+	16.18	16.35	2_5^+	19.00		4_5^+	22.58	11.93	2_5^+	6.49		2_5^+	11.12	9.00
3_1^+	12.13		3_1^+	4.30		6_1^+	10.03	8.78	3_1^+	9.25		3_1^+	5.245	5.43
3_2^+	13.58		3_2^+	19.03		6_2^+	12.73		3_2^+	9.33		3_2^+	11.52	13.43
3_3^+	16.83		3_3^+	24.97		6_3^+	15.28		3_3^+	12.97		3_3^+	15.41	
3_4^+	17.46		3_4^+	34.77		6_4^+	17.50		3_4^+	15.59		3_4^+	16.29	
3_5^+	21.46		3_5^+	41.71		6_5^+	19.08		3_5^+	16.11		3_5^+	18.25	
4_1^+	10.35	10.36	4_1^+	4.11	3.54				4_1^+	3.47	3.36	4_1^+	4.39	4.12
4_2^+	10.56	11.10	4_2^+	6.91	7.12				4_2^+	6.21	6.35	4_2^+	6.60	6.01
4_3^+	16.51	13.87	4_3^+	8.65					4_3^+	6.60		4_3^+	9.02	9.51
4_4^+	18.21	16.84	4_4^+	18.44					4_4^+	7.23		4_4^+	12.10	10.57
4_5^+	19.86	17.78	4_5^+	21.34					4_5^+	9.02		4_5^+	12.78	10.60
5_1^+	10.95		5_1^+	6.40					5_1^+	18.48		5_1^+	9.37	7.81
5_2^+	14.65		5_2^+	20.43					5_2^+	18.59		5_2^+	12.76	
5_3^+	15.19		5_3^+	26.53					5_3^+	22.29		5_3^+	14.03	
5_4^+	19.21		5_4^+	35.73					5_4^+	24.72		5_4^+	14.39	
5_5^+	22.37		5_5^+	42.61					5_5^+	25.48		5_5^+	15.50	
6_1^+	13.86	14.82	6_1^+	8.67					6_1^+	7.30		6_1^+	8.09	
6_2^+	21.40	16.28	6_2^+	11.32					6_2^+	9.81		6_2^+	8.67	
6_3^+	22.68	17.56	6_3^+	22.05					6_3^+	10.35		6_3^+	10.05	
6_4^+	25.80	19.31	6_4^+	24.87					6_4^+	11.13		6_4^+	10.81	
6_5^+	26.14	21.05	6_5^+	25.25					6_5^+	13.00		6_5^+	10.97	

$|F(R)|^2$ [20], where $F(R) \sim \exp(-aR^2)$ is the relative motion wave function. On the other hand, the expectation value of R satisfies $\langle R\rangle \sim \sqrt{n_\pi}$ when the SACM is mapped onto a geometrical picture [8] and this gives rise to the n_π dependence of the exponent. From this consideration, one expects a negative value for the parameter $B = -a$. The eigenvalues of the Casimir operators of the SU(3) groups are proportional to the square of the deformation [29,34]. A larger deformation corresponds to a more extended system and, thus, is also related to the relative distance of the clusters. The $SU_C(3)$ group describes the relative orientation of the nuclei [8] and large eigenvalues of the corresponding Casimir operator are related to an orientation which is less compact (more prolate), i.e., one can consider these operators as corrections to the overlap. Of course, these explanations are only qualitative and a more thorough understanding is desirable.

There is, however, a problem related to the expression in Eq. (25), exposed in detail in Ref. [6]: In the original ansatz the spectroscopic factor may have values greater than 1 as energy becomes large. In Ref. [6], a novel ansatz was proposed, which is identical to Ref. [31] for $\Delta n_\pi = 0$, 1, and 2, by which this problem may be circumvented.

This new ansatz for the spectroscopic factor is

$$\begin{aligned} S_{\mathrm{SU(3)}} = {} & \exp(F_1 + F_2) \\ & \times |\langle(\lambda_1,\mu_1)\kappa_1 L_1,(\lambda_2,\mu_2)\kappa_2 L_2||(\lambda_C,\mu_C)\kappa_C L_C\rangle_{\rho_C} \\ & \times \langle(\lambda_C,\mu_C)\kappa_C L_C,(n_\pi,0)1l||(\lambda,\mu)\kappa L\rangle_1|^2, \end{aligned} \tag{26}$$

where

$$\begin{aligned} F_1 = {} & [A + Bn_\pi + C\mathcal{C}_2(\lambda_1,\mu_1) + D\mathcal{C}_2(\lambda_2,\mu_2) + E\mathcal{C}_2(\lambda_c,\mu_c) \\ & + F\mathcal{C}_2(\lambda,\mu) + G\mathcal{C}_3(\lambda,\mu)] \end{aligned} \tag{27}$$

TABLE IV. The calculated and experimental values of the energy levels with negative parities.

L	$^{12}C+\alpha$		L	$^{14}C+\alpha$		L	$^{16}O+\alpha$		L	$^{18}O+\alpha$		L	$^{20}Ne+\alpha$	
	Calc.	Expt.		Calc.	Expt.		Calc.	Expt.		Calc.	Expt.		Calc.	Expt.
1^-_1	6.95	7.12	1^-_1	4.21	4.45	1^-_1	3.45	5.79	1^-_1	4.58	7.50	1^-_1	6.49	7.56
1^-_2	9.27	9.58	1^-_2	6.75	7.62	1^-_2	11.28	8.71	1^-_2	6.82	10.21	1^-_2	7.35	8.44
1^-_3	10.80	12.44	1^-_3	10.24	8.04	1^-_3	17.30	11.27	1^-_3	9.99		1^-_3	9.20	11.39
1^-_4	14.16	13.09	1^-_4	18.51		1^-_4	22.62	11.98	1^-_4	10.60		1^-_4	10.79	11.86
1^-_5	16.70	16.20	1^-_5	22.92		1^-_5	27.61		1^-_5	13.60		1^-_5	12.90	
2^-_1	9.10	8.81	2^-_1	5.28		3^-_1	4.63	5.62	2^-_1	4.62	5.15	2^-_1	6.57	8.86
2^-_2	10.72		2^-_2	10.56		3^-_2	11.31	9.12	2^-_2	10.00		2^-_2	8.50	
2^-_3	19.23		2^-_3	19.35		3^-_3	16.40	12.26	2^-_3	10.03		2^-_3	9.62	
2^-_4	22.65		2^-_4	26.63		3^-_4	20.78	12.20	2^-_4	13.82		2^-_4	11.42	
2^-_5	24.21		2^-_5	33.87		3^-_5	24.72	12.40	2^-_5	18.04		2^-_5	13.19	
3^-_1	6.01	6.13	3^-_1	5.41	0.10	5^-_1	6.47	8.45	3^-_1	9.74	10.85	3^-_1	6.93	7.61
3^-_2	7.99	11.6	3^-_2	7.80	8.28	5^-_2	10.94		3^-_2	11.97		3^-_2	8.021	8.36
3^-_3	9.71	13.13	3^-_3	10.66		5^-_3	14.53		3^-_3	14.99		3^-_3	9.33	11.16
3^-_4	12.26	13.26	3^-_4	11.68		5^-_4	17.50		3^-_4	15.14		3^-_4	10.49	11.60
3^-_5	15.62	14.10	3^-_5	19.31		5^-_5	19.89		3^-_5	15.84		3^-_5	10.87	12.01
4^-_1	13.52		4^-_1	8.36					4^-_1	7.14		4^-_1	6.95	
4^-_2	22.23		4^-_2	13.15					4^-_2	12.44		4^-_2	9.32	
4^-_3	24.39		4^-_3	21.70					4^-_3	12.45		4^-_3	10.14	
4^-_4	26.87		4^-_4	28.72					4^-_4	16.28		4^-_4	11.17	
4^-_5	28.71		4^-_5	35.89					4^-_5	18.75		4^-_5	11.75	
5^-_1	5.69	14.66	5^-_1	7.61	7.86				5^-_1	19.03		5^-_1	7.54	10.03
5^-_2	7.57	18.40	5^-_2	9.69	8.13				5^-_2	21.26		5^-_2	8.74	
5^-_3	8.81	18.60	5^-_3	12.47					5^-_3	24.06		5^-_3	10.12	
5^-_4	13.67	19.25	5^-_4	14.30					5^-_4	24.39		5^-_4	11.14	
5^-_5	15.91	20.54	5^-_5	20.76					5^-_5	25.20		5^-_5	11.38	
6^-_1	17.86		6^-_1	13.24					6^-_1	11.09		6^-_1	7.47	
6^-_2	27.01		6^-_2	17.23					6^-_2	16.23		6^-_2	9.54	
6^-_3	30.89		6^-_3	25.35					6^-_3	16.31		6^-_3	10.53	
6^-_4	31.29		6^-_4	32.02					6^-_4	20.17		6^-_4	11.45	
6^-_5	34.28		6^-_5	39.06					6^-_5	22.44		6^-_5	12.19	

TABLE V. $B(E2)$ transition probabilities for the systems $^{12}C+\alpha$, $^{14}C+\alpha$, and $^{16}C+\alpha$.

$L' \to L$	$^{12}C+\alpha$		$L' \to L$	$^{14}C+\alpha$		$L' \to L$	$^{16}O+\alpha$	
	Calc.	Expt.		Calc.	Expt.		Calc.	Expt.
$2^+_1 \to 0^+_1$	7.49×10^{-3}	3.1(1)	$2^+_1 \to 0^+_1$	3.80	3.32(9)	$0^+_2 \to 2^+_1$	2.15	3.6
$2^+_1 \to 0^+_2$	30.74	27(3)	$2^+_1 \to 0^+_2$	6.49×10^{-3}		$0^+_2 \to 2^+_2$	146.70	
$2^+_1 \to 0^+_3$	0.15		$2^+_1 \to 0^+_3$	7.76×10^{-3}		$0^+_2 \to 2^+_3$	0.33	
$2^+_2 \to 0^+_1$	7.64×10^{-6}	0.031(3)	$2^+_2 \to 0^+_1$	1.22	1.3(2)	$2^+_1 \to 0^+_1$	21.08	20.3(10)
$2^+_2 \to 0^+_2$	0.03		$2^+_2 \to 0^+_2$	3.37×10^{-3}		$2^+_1 \to 0^+_2$	0.43	
$2^+_2 \to 0^+_3$	136.33		$2^+_2 \to 0^+_3$	9.72×10^{-6}		$2^+_1 \to 0^+_3$	1.83×10^{-4}	
$2^+_3 \to 0^+_1$	0.22	1.5(5)	$2^+_3 \to 0^+_1$	0.00	2.15(11)	$5^-_1 \to 3^-_1$	34.34	27(6)
$2^+_3 \to 0^+_2$	5.49		$2^+_3 \to 0^+_2$	0.17	23(15)	$5^-_1 \to 3^-_2$	4.87	
$2^+_3 \to 0^+_3$	0.00		$2^+_3 \to 0^+_3$	6.27×10^{-5}		$5^-_1 \to 3^-_3$	0.11	
$4^+_1 \to 2^+_1$	41.28	65(6)	$2^+_4 \to 0^+_1$	9.12×10^{-3}	0.9(3)			
$4^+_1 \to 2^+_2$	10.62		$2^+_4 \to 0^+_2$	1.06×10^{-4}				
$4^+_1 \to 2^+_3$	4.77		$2^+_4 \to 0^+_3$	4.86				
$4^+_2 \to 2^+_1$	0.97	1(3)	$4^+_1 \to 2^+_1$	5.02	1.19(6)			
$4^+_2 \to 2^+_2$	179.12		$4^+_1 \to 2^+_2$	0.06				
$4^+_2 \to 2^+_3$	0.29		$4^+_1 \to 2^+_3$	0.01				
$1^-_1 \to 3^-_1$	17.37	21(5)	$4^+_2 \to 2^+_1$	0.67				
$1^-_1 \to 3^-_2$	0.22		$4^+_2 \to 2^+_2$	1.93	2.2(6)			
$1^-_1 \to 3^-_3$	0.40×10^{-5}		$4^+_2 \to 2^+_3$	1.13×10^{-3}				

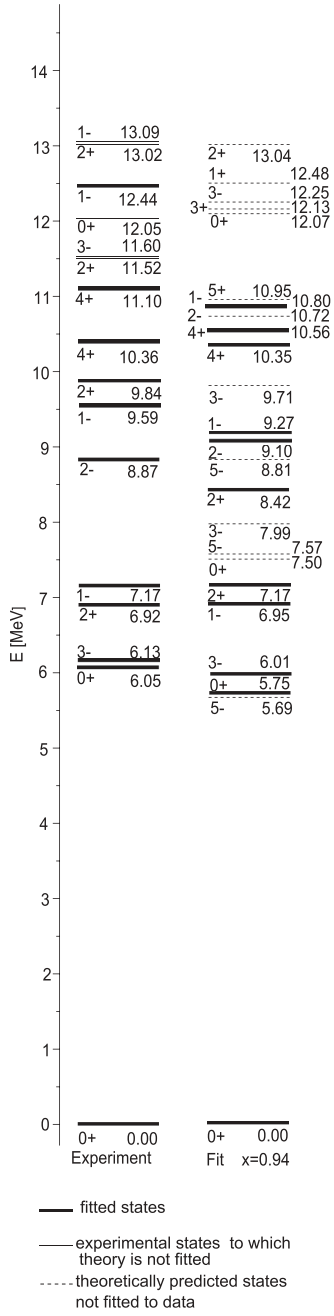

FIG. 1. Spectrum of the cluster system $^{12}C + \alpha \rightarrow {}^{16}O$. Thick solid lines represent states in the ^{16}O nucleus for which $^{12}C(\alpha, \gamma)^{16}O$ is a populating reaction. On the experimental side, thin solid lines are not included in the fit and dashed lines represent states which are, in addition, predicted by the theory.

and

$$F_2 = -F_1 \frac{\Delta n_\pi (\Delta n_\pi - 1)(\Delta n_\pi - 2)}{n_\pi^3} + H \frac{(n_0+2)^3(\Delta n_\pi - 1)}{n_\pi^4} \frac{\Delta n_\pi}{n_\pi}. \quad (28)$$

Both Eqs. (25) and (26) are diagonal in a SU(3) basis, which is the reason that they are not written in terms of operators. When mixing is included, the spectroscopic factor calculated

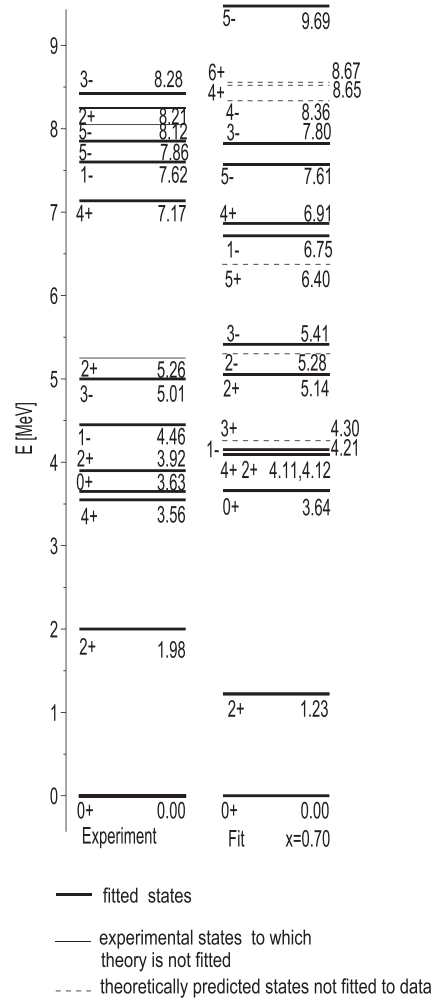

FIG. 2. Spectrum of the cluster system $^{14}C + \alpha \rightarrow {}^{18}O$. Thick solid lines represent states in the ^{18}O nucleus for which $^{14}C(\alpha, \gamma)^{18}O$ is a populating reaction. On the experimental side, thin solid lines are not included in the fit and dashed lines represent states which are, in addition, predicted by the theory.

will deviate from SU(3), such that it acquires the form

$$S = \sum_i |c_i|^2 S_{\mathrm{SU(3)},i}, \quad (29)$$

where c_i are the coefficients of a given state within the SU(3) basis and i is a shorthand notation for all SU(3) quantum numbers. (Note that in Ref. [6] we committed the error of not squaring the coefficients.)

V. NUMERICAL STUDIES

A. Methodology

In this section we apply the model to the systems $^{12}C + \alpha \rightarrow {}^{16}O$, $^{14}C + \alpha \rightarrow {}^{18}O$, $^{16}O + \alpha \rightarrow {}^{20}Ne$, $^{18}O + \alpha \rightarrow {}^{22}Ne$, and $^{20}Ne + \alpha \rightarrow {}^{24}Mg$. These are core+$\alpha$ nuclei and play an important role in astrophysics, known as *secondary* α *process*, as mentioned in the Introduction. Some of these systems have already been discussed in Refs. [3,4]. However,

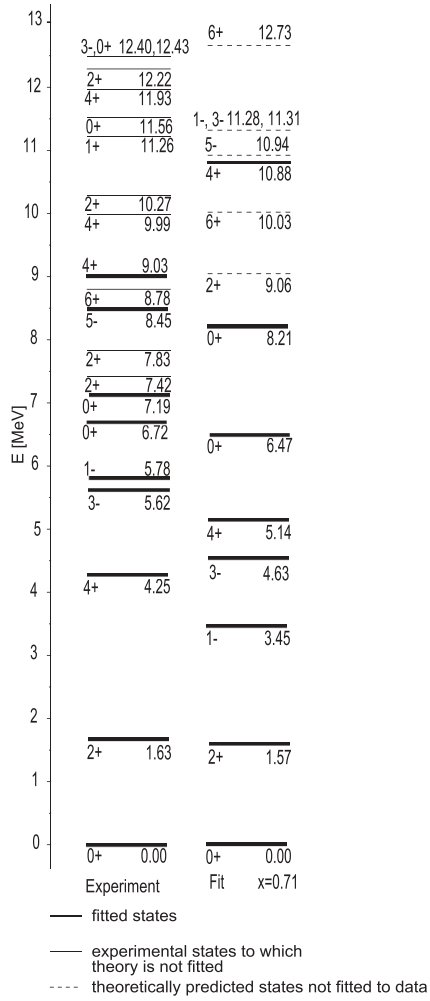

FIG. 3. Spectrum of the cluster system $^{16}\mathrm{O} + \alpha \rightarrow {}^{20}\mathrm{Ne}$. Thick solid lines represent states in the ^{20}Ne nucleus for which $^{16}\mathrm{O}(\alpha, \gamma)^{20}\mathrm{Ne}$ is a populating reaction. On the experimental side, thin solid lines are not included in the fit and dashed lines represent states which are, in addition, predicted by the theory.

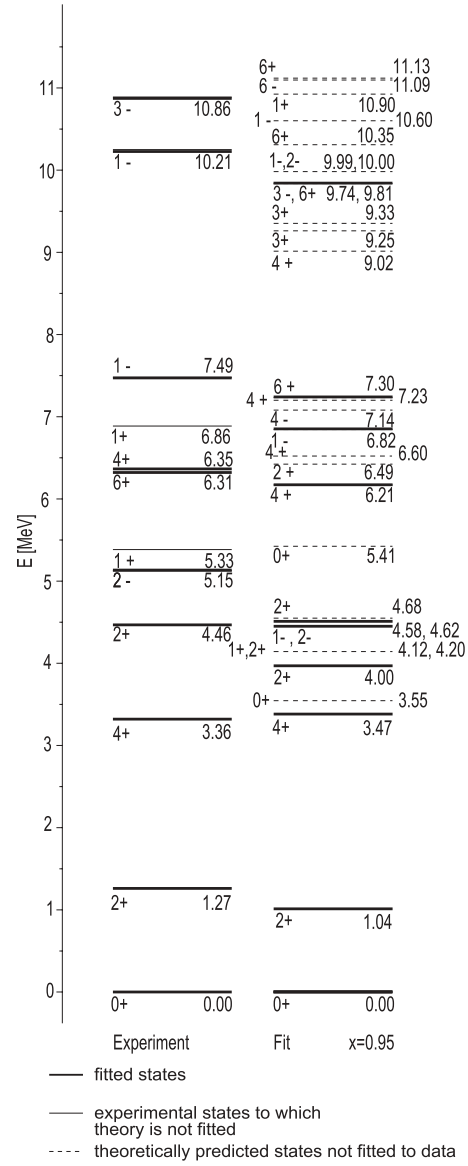

FIG. 4. Spectrum of the cluster system $^{18}\mathrm{O} + \alpha \rightarrow {}^{22}\mathrm{Ne}$. Thick solid lines represent states in the ^{22}Ne nucleus for which $^{18}\mathrm{O}(\alpha, \gamma)^{22}\mathrm{Ne}$ is a populating reaction. On the experimental side, thin solid lines are not included in the fit and dashed lines represent states which are, in addition, predicted by the theory.

in each case a Hamiltonian of a single dynamic symmetry was chosen, which we abandon in our present analysis, permitting the reproduction of transitions which belong to different SU(3) irreps. In Ref. [6] the $^{14}\mathrm{C} + \alpha$ and $^{20}\mathrm{Ne} + \alpha$ systems were investigated, restricting to the SU(3) dynamical symmetry, which set transitions between different irreps to zero, though experiment indicates the existence of such transitions.

All spectral data used herein are taken from the National Nuclear Data Center data tables [35]. These tables also list the populating reactions of a given state. Only those states populated by the considered clusterization are taken into account. Problems of identification may arise when a state has an overlap with an α process, but such has not been observed in the corresponding experiment due to lack of sensitivity. Due to this, fewer states appear at low energy than in fits that include states not seen in direct reaction experiments of the type $A(\alpha, \gamma)B$. We will come back to this in the discussion on the spectrum of ^{20}Ne, where one particular example is discussed.

The parameters of the Hamiltonian and the correction factor p_{e2} for the $B(E2)$ transitions have been adjusted to the spectrum and quadrupole-transition values according to a three-step fitting procedure. First, the SU(3) shell-model space is constructed. Initially, this is done in the case where only the valence shell is open. We then consider all $1\hbar\omega$ excitations and determine the SU(3) irreps. From the obtained list we subtract all states also obtained by multiplying the SU(3) irreps of the $0\hbar\omega$ excitation with $(1, 0)$ representing spurious center-of-mass motion. We then consider all $2\hbar\omega$ excitations, providing a further list of SU(3) irreps, and from this we subtract all irreps obtained by multiplying the irreps

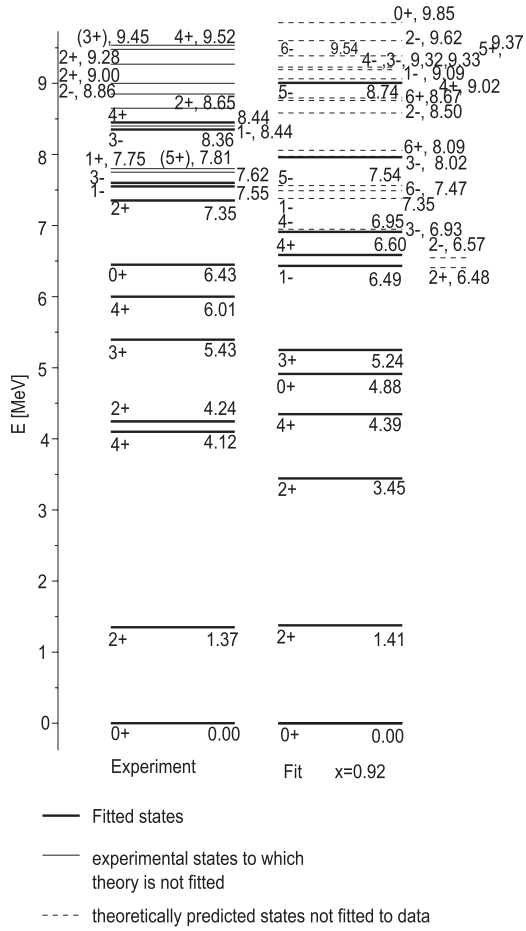

FIG. 5. Spectrum of the cluster system $^{20}\mathrm{Ne}+\alpha \rightarrow {}^{24}\mathrm{Mg}$. Thick solid lines represent states in the ^{24}Mg nucleus for which $^{20}\mathrm{Ne}(\alpha,\gamma)^{24}\mathrm{Mg}$ is a populating reaction. On the experimental side, thin solid lines are not included in the fit and dashed lines represent states which are, in addition, predicted by the theory.

of the $0\hbar\omega$ excitations with $(2, 0)$ and all $1\hbar\omega$ excitations with $(1, 0)$, again eliminating spurious center-of-mass motion. This procedure is repeated for higher $\hbar\omega$ excitations. Parallel to this, we calculate the direct product $(\lambda_1, \mu_1) \otimes (\lambda_2, \mu_2) \otimes (n_\pi, 0)$, producing a large list of SU(3) irreps. This list is compared to the SU(3) shell-model content, and our space is made of all states in the former which overlap with the latter. With this, the Pauli exclusion principle is observed.

In a second step, all relevant matrix elements for the interaction terms and electro-magnetic transition operators are constructed. This step uses the microscopic model space calculated in the first step. In a third and last step, the Hamiltonian is constructed and diagonalized. Parameter values may be either sought by fit to data or specified.

In fitting the parameters, care has to be taken; if used blindly, the program tends to jump to the SO(4) dynamical limit ($x = 0$ and $y = 1$). The lowest-lying states will then exhibit a nonphysical structure, where the average number of π bosons will jump from $n_\pi = N$ (i.e., the maximal allowed number) to $n_\pi = n_0$ and so on. This is nonphysical as N is a cutoff, and when the lowest states belong to a maximal n_π, no convergence of the results can be claimed. The numerical

TABLE VI. $B(E2)$ transition probabilities for the systems $^{18}\mathrm{O}+\alpha$ and $^{20}\mathrm{Ne}+\alpha$.

$L' \rightarrow L$	$^{18}\mathrm{O}+\alpha$		$L' \rightarrow L$	$^{20}\mathrm{Ne}+\alpha$	
	Calc.	Expt.		Calc.	Expt.
$2_1^+ \rightarrow 0_1^+$	11.89	12.5(5)	$0_2^+ \rightarrow 2_1^+$	1.25	
$2_1^+ \rightarrow 0_2^+$	0.050		$0_2^+ \rightarrow 2_2^+$	3.50	8.9(14)
$2_1^+ \rightarrow 0_3^+$	9.59×10^{-6}		$0_2^+ \rightarrow 2_3^+$	51.35	
$2_3^+ \rightarrow 0_1^+$	1.12	>0.26	$2_1^+ \rightarrow 0_1^+$	15.42	21.5(10)
$2_3^+ \rightarrow 0_2^+$	0.034		$2_1^+ \rightarrow 0_2^+$	0.25	
$2_3^+ \rightarrow 0_3^+$	2.08×10^{-6}		$2_1^+ \rightarrow 0_3^+$	0.02	
$2_2^+ \rightarrow 2_1^+$	0.16	>0.21	$2_2^+ \rightarrow 0_1^+$	1.78	1.94(19)
$2_2^+ \rightarrow 2_3^+$	0.20		$2_2^+ \rightarrow 0_2^+$	0.70	
$6_1^+ \rightarrow 4_1^+$	14.45	13.7(17)	$2_2^+ \rightarrow 0_3^+$	0.02	
$6_1^+ \rightarrow 4_2^+$	0.30		$2_1^+ \rightarrow 2_2^+$	5.49	
$6_1^+ \rightarrow 4_3^+$	0.13		$2_1^+ \rightarrow 2_3^+$	0.05	

reason behind this is that in the SU(3) dynamical limit, the sequence of states in a band behaves as $L(L + 1)$, while in the SO(4) case this band structure is deformed. In experimental spectra, the dependence of the states on L is never truly $L(L + 1)$ though may be approximately so. Thus, in order to reproduce the correct L dependence within a band, the program prefers to jump to the SO(4) dynamical limit. One can reduce this tendency by allowing *only* one large angular-momentum state from the ground-state band (e.g., 4_1^+ or 6_1^+), and only the band head of the other bands in the list of experimental data. This method will work less when the identification of bands is not as clear or when the order of spin states is unusual (as in the negative-parity bands in the oxygen isotopes). All FORTRAN programs that perform the above are available on request.

For nuclei in the *sd* shell, one expects that the SU(3) dynamical symmetry is better realized than the others considered, and so we begin at this limit ($x = 1$ and $y = 1$). Normally, this yields good results, with the exception that some transition values, which belong to transitions between different SU(3) irreps, are calculated to be zero, while in experiment they are not. This is corrected by seeking a value of x near, but not exactly, 1, which allows mixing between different SU(3) irreps. The affected transition values are then well reproduced. We verify at the end of each step that the structure of the low-lying states contain only low excitations in n_π and do not approach the largest possible number, N.

After having fitted the parameters, we calculate further states in the spectrum and additional $B(E2)$ transition values. In addition, we determine the $B(E1)$ and $B(M1)$ transitions. As it is relevant to astrophysics, we have also calculated spectroscopic factors of the first states in each system. The experimental values for the spectroscopic factors were taken from Refs. [36–41].

In the spectral plots presented, we do not use the standard presentation in terms of bands, though in the SU(3) dynamical limit, which is nearly realized in *sd*-shell nuclei, one can associate a good K quantum number with each state. The reason for this choice is that the bands do not follow an $L(L + 1)$ rule, so much so that the order of spin states is

TABLE VII. $B(M1)$ transition probabilities for the systems $^{12}C + \alpha$ and $^{14}C + \alpha$.

$L' \to L$	$^{12}C + \alpha$		$L' \to L$	$^{14}C + \alpha$	
	Calc.	Expt.		Calc.	Expt.
$2_2^+ \to 2_1^+$	1.03×10^{-5}	0.0042(8)	$2_2^+ \to 2_1^+$	8.20×10^{-4}	0.014(2)
$2_2^+ \to 2_2^+$	1.68		$2_2^+ \to 2_2^+$	0.90	
$2_2^+ \to 2_3^+$	7.26×10^{-5}		$2_2^+ \to 2_3^+$	2.05×10^{-8}	
$2_3^+ \to 2_1^+$	0.04	0.014(4)	$2_3^+ \to 2_1^+$	10.60×10^{-4}	
$2_3^+ \to 2_2^+$	2.03×10^{-5}		$2_3^+ \to 2_2^+$	1.17×10^{-8}	0.111(8)
$2_3^+ \to 2_3^+$	1.39		$2_4^+ \to 2_1^+$	8.25×10^{-9}	
$1_4^- \to 1_1^-$	4.82×10^{-8}	0.31(9)	$2_4^+ \to 2_2^+$	1.71×10^{-6}	0.0072(30)
$1_4^- \to 1_2^-$	9.89×10^{-4}		$2_4^+ \to 2_3^+$	2.73×10^{-10}	
$1_4^- \to 1_3^-$	2.37×10^{-6}		$4_2^+ \to 4_1^+$	3.74×10^{-4}	0.071(16)
			$4_2^+ \to 4_3^+$	5.86×10^{-7}	
			$1_2^- \to 1_1^-$	2.15×10^{-3}	
			$1_2^- \to 1_3^-$	1.93×10^{-4}	
			$1_3^- \to 1_1^-$	0.02	0.063(13)
			$1_3^- \to 1_2^-$	1.47×10^{-4}	0.07(7)

inverted in some bands. An example of this is $^{16,18}O$. This behavior can be reproduced by a spin and n_π dependence in the moment of inertia. Therefore, it is difficult to associate this with a rotational band, and, thus, we prefer a simple sequential list of states. Another reason concerns how one may reconstruct a band without using a theoretical association with quantum numbers: one starts with a high-angular-momentum state and connects it with a lower-angular-momentum state with which it shares the largest $B(E2)$ value. This is continued until the lowest-angular-momentum state is reached. In nuclei with a pure SU(3) dynamical symmetry, this results in bands with the usual $L(L+1)$ behavior. However, in some cases, discussed here, this identification produces bands with inverted spin and sometimes the $B(E2)$ value is of similar size for two of the lowest-angular-momentum states, which is due to mixing, i.e., even being near the SU(3) dynamical limit, mixing can be of importance.

B. Results and discussion

Though the structure of the Hamiltonian used is quite general, in the systems discussed in this paper the optimal value for mixing parameter y turns out to be 1. Nevertheless, for other systems, the more general Hamiltonian might be of importance, i.e., the value of y could differ from 1 (hence its inclusion in the development).

In Table II, the values for the parameters, fitted to experimental data, are listed. Looking to the parameter p_{e2}, it being a guide to the quality of the model, we see that the largest deviation from 1 was found for $^{14}C + \alpha$, though the estimation is only a factor of 3 out. This shows us that the $M1$ and $E1$ transitions, which were not adjusted, may be off by the same factor in that system.

In Tables III and IV we compare calculated energy values to experiment. The states with positive parity are listed in Table III while those with negative parity are listed in Table IV. In Figs. 1 to 5, the spectra of the nuclei ^{16}O, ^{18}O, ^{20}Ne, ^{22}Ne, and ^{24}Mg are plotted, comparing model calculations with experiment. Agreement is quite good.

One area of difficulty is in reproducing the sequence 3^-, 1^-, and 2^- in the negative-parity band of $^{12}C + \alpha$. (In the other nuclei the lowest negative-parity states are quite close compared to states within a positive-parity band.) The problem was overcome with the introduction of interaction terms which

TABLE VIII. $B(M1)$ transition probabilities for the systems $^{16}O + \alpha$ and $^{18}O + \alpha$.

$L' \to L$	$^{16}O + \alpha$		$L' \to L$	$^{18}O + \alpha$	
	Calc.	Expt.		Calc.	Expt.
$2_3^+ \to 2_1^+$	5.06×10^{-4}	$2.3 \times 10^{-3}(3)$	$1_1^+ \to 0_1^+$	0.075	0.088(19)
$2_3^+ \to 2_2^+$	3.13×10^{-4}		$1_1^+ \to 0_2^+$	0.094	
$2_4^+ \to 2_1^+$	5.85×10^{-5}		$1_1^+ \to 0_3^+$	4.40×10^{-8}	
$2_4^+ \to 2_2^+$	5.40×10^{-7}	0.64(8)	$1_2^+ \to 0_1^+$	4.07×10^{-5}	0.21(5)
$2_4^+ \to 2_3^+$	3.07×10^{-5}	$2.6 \times 10^{-2}(7)$	$1_2^+ \to 0_2^+$	1.21×10^{-6}	
$4_4^+ \to 4_1^+$	6.58×10^{-4}	2.2×10^{-3}	$1_2^+ \to 0_3^+$	0.08	
$4_4^+ \to 4_2^+$	4.61×10^{-6}				
$4_4^+ \to 4_3^+$	2.35×10^{-5}				
$3_2^- \to 3_1^-$	7.74×10^{-4}				
$3_2^- \to 3_3^-$	7.37×10^{-4}				

depend on the angular momentum L and on $\Delta \boldsymbol{n}_\pi$ [see Eqs. (2) and (3)]. Due to the parity and n_π dependence of the moment of inertia, a 5^- state in ^{16}O (belonging to a $3\hbar\omega$ excitation [7]) is calculated as having quite a low energy. This is due to a large positive a_L parameter in the moment of inertia which is multiplied by $(-1)^L$, i.e., bringing down negative-parity states with a large angular momentum. This might be a peculiarity of the fit or may indicate a general behavior of low-lying negative-parity states with large spin. However, the value of a_L is important in reproducing the spin-sequence 3^-, 1^-, and 2^-. For the other systems, a_L is either smaller or negative.

As mentioned before, we include in the fit only states which are seen in a direct (α, γ) reaction. An example, as discussed also in a supersymmetric formulation of the cluster model [42, 43], is that the first 3^- state in ^{20}Ne is at 7.156 MeV, but we exclude it because it does not appear in the list of states observed in the mentioned reaction. Thus, the first 3^- state we include is at 5.62 MeV, as listed in Ref. [35]. Similar considerations apply for the other cluster systems considered in this paper.

In Tables V and VI, the $B(E2)$-transition values, as calculated in the model, are compared to experiment. The same is listed in Tables VII, VIII, and IX for $M1$ transitions and in Table X for $E1$ transitions. In general, the $B(E2)$ values are well reproduced, which, considered alongside the good reproduction of the spectra, allows for confidence in the SACM.

The exceptions to this agreement are the $2_1^+ \to 0_1^+$ transition in $^{12}\mathrm{C}+\alpha$ and the transitions in $^{14}\mathrm{C}+\alpha$ from 4_1^+ to 2_3^+ and from 2_3^+ to 0_2^+, compared to the ground-state band transitions, which are extremely strong in experiment. In $^{12}\mathrm{C}+\alpha$ this deviation might be due to the low-lying 0^+ excited state and in $^{14}\mathrm{C}+\alpha$ this indicates a different structure of these states, being strongly deformed. One possibility [6] is that these states are localized in a highly deformed minimum and are out of the scope of the model Hamiltonian used here. In this case, the reproduced spectrum of ^{18}O has to be taken with care, excluding those states. The $M1$ transitions are not so well reproduced, also indicating a limit to the applicability of the model. The situation is much better for the $E1$ transitions, though data of appropriate clusterization was available only for the $^{14}\mathrm{C}+\alpha$ system.

In Ref. [6], the fitting of $^{14}\mathrm{C}+\alpha$ was performed in the SU(3) limit, i.e., $x = 1$, and as such, this was a system where several transitions were erroneously found to be zero, as they involved different SU(3) irreps. Allowing x to differ from 1, as discussed above, the results are now nonzero and reproduce the experiment quite well.

Considering the difficulty of simultaneously describing a spectrum and $E2$, $E1$, and $M1$ transitions with a single model, and also taking into account that, for the latter two, only the

TABLE IX. $B(M1)$ transition probabilities for the system $^{20}\mathrm{Ne}+\alpha$.

$L' \to L$	$^{20}\mathrm{Ne}+\alpha$	
	Calc.	Expt.
$1_3^+ \to 0_1^+$	3.47×10^{-4}	0.0078(20)
$1_3^+ \to 0_2^+$	5.33×10^{-3}	
$1_3^+ \to 0_1^+$	6.67×10^{-3}	

TABLE X. $B(E1)$ transition probabilities for the system $^{14}\mathrm{C}+\alpha$. Only the values of this system are listed, as these are the largest. For the other systems the values determined are very small, which agrees with experiment (either also very small or not observed).

$L' \to L$	$^{14}\mathrm{C}+\alpha$	
	Calc.	Expt.
$2_3^+ \to 1_1^-$	1.74×10^{-5}	0.0082(8)
$2_3^+ \to 1_2^-$	1.35×10^{-6}	
$2_3^+ \to 1_3^-$	0.46	
$2_4^+ \to 1_1^-$	4.1×10^{-4}	0.0050(11)
$2_4^+ \to 1_2^-$	0.34	
$2_4^+ \to 1_3^-$	8.41×10^{-4}	
$4_2^+ \to 3_1^-$	8.91×10^{-4}	0.0029(8)
$4_2^+ \to 3_2^-$	6.38×10^{-6}	
$4_2^+ \to 3_3^-$	0.39	
$1_2^- \to 0_1^+$	0.53	0.000 46(11)
$1_2^- \to 0_2^+$	8.32×10^{-6}	
$1_2^- \to 0_3^+$	0.21	
$1_4^- \to 0_1^+$	3.39×10^{-3}	
$1_4^- \to 0_2^+$	8.29×10^{-5}	0.000 28(8)
$1_4^- \to 0_3^+$	1.58×10^{-5}	
$1_3^- \to 1_1^+$	6.16×10^{-5}	0.000 70(17)
$1_3^- \to 1_2^+$	2.63×10^{-6}	
$1_3^- \to 1_3^+$	8.73×10^{-9}	
$1_1^- \to 2_1^+$	2.57×10^{-6}	0.000 41(10)
$1_1^- \to 2_2^+$	17.9×10^{-3}	0.0035(11)
$1_1^- \to 2_3^+$	2.90×10^{-5}	
$1_3^- \to 2_1^+$	2.59×10^{-4}	0.0072(15)
$1_3^- \to 2_2^+$	2.79×10^{-6}	
$1_3^- \to 2_3^+$	0.78	0.0043(14)
$3_1^- \to 2_1^+$	4.67×10^{-3}	0.000 57(23)
$3_1^- \to 2_2^+$	3.11×10^{-5}	0.0025(11)
$3_1^- \to 2_3^+$	5.35×10^{-3}	
$3_2^- \to 2_1^+$	0.73	
$3_2^- \to 2_2^+$	3.54×10^{-7}	
$3_2^- \to 2_3^+$	7.52×10^{-5}	0.014(5)
$3_1^- \to 4_1^+$	2.67×10^{-4}	0.000 36(15)
$3_1^- \to 4_2^+$	1.15×10^{-3}	
$3_1^- \to 4_3^+$	7.07×10^{-5}	
$3_2^- \to 4_1^+$	0.65	0.0061(16)
$3_2^- \to 4_2^+$	8.21×10^{-6}	
$3_2^- \to 4_3^+$	9.38×10^{-8}	
$5_1^- \to 4_1^+$	8.48×10^{-3}	>0.0009
$5_1^- \to 4_2^+$	1.61×10^{-5}	
$5_1^- \to 4_3^+$	6.29×10^{-3}	
$5_1^- \to 4_4^+$	1.40×10^{-3}	
$5_1^- \to 4_5^+$	2.52×10^{-5}	
$5_2^- \to 4_1^+$	0.82	0.0061(11)
$5_2^- \to 4_2^+$	8.10×10^{-7}	
$5_2^- \to 4_3^+$	1.44×10^{-4}	

TABLE XI. Spectroscopic factors for positive-parity levels. The indices a, b, and c correspond to Refs. [38,40,41], respectively.

L	$^{12}C+\alpha$		L	$^{14}C+\alpha$		L	$^{16}O+\alpha$		L	$^{18}O+\alpha$		L	$^{20}Ne+\alpha$	
	Calc.	Expt.		Calc.	Expt.		Calc.	Expt.		Calc.	Expt.		Calc.	Expt.
0_1^+	0.160	0.42[a]	0_1^+	0.176		0_1^+	0.195	0.15[a]	0_1^+	0.068		0_1^+	0.052	
0_2^+	0.260		0_2^+	0.196		0_2^+	0.108		0_2^+	0.123		0_2^+	0.063	
0_3^+	0.211		0_3^+	0.100		0_3^+	0.060		0_3^+	0.014		0_3^+	0.064	
0_4^+	0.150		0_4^+	0.116		0_4^+	0.030	0.70[c]	0_4^+	0.027		0_4^+	0.038	
0_5^+	0.147		0_5^+	0.044		0_5^+	0.013		0_5^+	0.058		0_5^+	0.026	
1_1^+	0.778		1_1^+	0.121		2_1^+	0.190	0.11[a]	1_1^+	0.063		1_1^+	0.025	
1_2^+	0.274		1_2^+	0.060		2_2^+	0.108		1_2^+	0.016		1_2^+	0.020	
1_3^+	0.447		1_3^+	0.026		2_3^+	0.060		1_3^+	0.027		1_3^+	0.015	
1_4^+	0.124		1_4^+	0.011		2_4^+	0.030		1_4^+	0.008		1_4^+	0.014	
1_5^+	0.207		1_5^+			2_5^+	0.014		1_5^+	0.014		1_5^+	0.010	
2_1^+	0.172	1.10[a]	2_1^+	0.171		4_1^+	0.176	0.12[a]	2_1^+	0.052		2_1^+	0.018	
2_2^+	0.202		2_2^+	9.78×10^{-5}		4_2^+	0.104		2_2^+	0.030		2_2^+	0.005	
2_3^+	0.089		2_3^+	0.170		4_3^+	0.065		2_3^+	0.001		2_3^+	0.014	
2_4^+	0.089		2_4^+	0.097		4_4^+	0.039	0.95[c]	2_4^+	0.100		2_4^+	0.004	
2_5^+	0.028		2_5^+	0.104		4_5^+	0.020		2_5^+	0.013		2_5^+	0.016	
3_1^+	0.763		3_1^+	0.168		6_1^+	0.113	0.085[a,c]	3_1^+	0.062		3_1^+	0.036	
3_2^+	0.269		3_2^+	0.096		6_2^+	0.082		3_2^+	0.051		3_2^+	0.046	
3_3^+	0.635		3_3^+	0.120		6_3^+	0.067		3_3^+	0.071		3_3^+	0.015	
3_4^+	0.199		3_4^+	0.043		6_4^+	0.050	0.33[c]	3_4^+	0.0002		3_4^+	0.019	
3_5^+	0.438	0.28[a]	3_5^+	0.059		6_5^+	0.026		3_5^+	0.016		3_5^+	0.018	
4_1^+	0.036		4_1^+	0.160					4_1^+	0.024		4_1^+	0.0006	
4_2^+	0.169		4_2^+	0.002					4_2^+	0.065		4_2^+	0.020	
4_3^+	0.178		4_3^+	0.106					4_3^+	0.007		4_3^+	0.009	
4_4^+	0.079		4_4^+	0.092					4_4^+	0.074		4_4^+	0.002	
4_5^+	0.051		4_5^+	0.0006					4_5^+	0.011		4_5^+	0.005	
5_1^+	0.254		5_1^+	0.165					5_1^+	0.057		5_1^+	0.023	
5_2^+	0.188		5_2^+	0.094					5_2^+	0.050		5_2^+	0.012	
5_3^+	0.602		5_3^+	0.118					5_3^+	0.066		5_3^+	0.012	
5_4^+	0.417		5_4^+	0.042					5_4^+	0.001		5_4^+	0.020	
5_5^+	0.115		5_5^+	0.058					5_5^+	0.015		5_5^+	0.014	
6_1^+	0.138	0.28[a,b]	6_1^+	0.139					6_1^+	0.003		6_1^+	0.005	
6_2^+	0.128		6_2^+	0.008					6_2^+	0.085		6_2^+	0.008	
6_3^+	0.022		6_3^+	0.082					6_3^+	0.027		6_3^+	0.009	
6_4^+	0.017		6_4^+	0.003					6_4^+	0.042		6_4^+	0.016	
6_5^+	0.069		6_5^+	0.046					6_5^+	0.008		6_5^+	0.018	

geometric estimate of the effective charge was used, one can be satisfied with the results obtained.

Tables XI and XII list the spectroscopic factors of the first five states for each J^π combination, with $J = 0, 1, 2, 3, 4, 5, 6$ for the positive-parity states and $J = 1, 2, 3, 4, 5, 6$ for the negative. No 0^- appears in the model space, and these are not observed in fusion reactions which include an α particle.

One has to be careful with the experimentally deduced values because, usually, theoretical penetration models are involved and, thus, the result is model dependent. The ratio of the experimentally measured differential cross section to that of the theoretically deduced value within a penetration calculation is defined as the *experimental* measured spectroscopic factor. A difference of orders of magnitude may arise due to the link to this specific model, which does not take into account other possible structure effects such as those of the formation of a cluster.

The theoretically determined spectroscopic factors listed in these tables can be used in calculations of fusion cross sections.

VI. CONCLUSIONS

The SACM was applied to several *secondary* α *fusion processes*. The Hamiltonian used is an extended version of those formerly used and includes terms which reproduce well the distinct behavior of states in negative-parity bands, compared to states within positive-parity bands.

The matrix elements of all interaction terms and $E2$, $E1$, and $M1$ transition operators have been listed and corresponding transition values calculated. For all transition operators, the effective charges were estimated geometrically and for the $E2$ transition proved to be close to the adjusted $E2$ effective charges. The calculations were performed without restricting to specific dynamical symmetry limits and instead

TABLE XII. Spectroscopic factors for negative-parity levels. The indices c, d, e, and f correspond to Refs. [36–39], respectively.

L	$^{12}C+\alpha$		L	$^{14}C+\alpha$		L	$^{16}O+\alpha$		L	$^{18}O+\alpha$		L	$^{20}Ne+\alpha$	
	Calc.	Expt.		Calc.	Expt.		Calc.	Expt.		Calc.	Expt.		Calc.	Expt.
1^-_1	0.048	0.5[d]	1^-_1	0.007		1^-_1	0.117	1.03[d]	1^-_1	0.002		1^-_1	0.006	
1^-_2	0.017		1^-_2	0.129		1^-_2	0.071		1^-_2	0.037		1^-_2	0.025	
1^-_3	0.183		1^-_3	0.126		1^-_3	0.042		1^-_3	0.006		1^-_3	0.020	
1^-_4	0.136		1^-_4	0.003		1^-_4	0.022		1^-_4	0.073		1^-_4	0.021	
1^-_5	0.107		1^-_5	0.067		1^-_5	0.008		1^-_5	0.009		1^-_5	0.019	
2^-_1	0.869		2^-_1	0.285		3^-_1	0.112	0.87[d]	2^-_1	0.024		2^-_1	0.001	
2^-_2	0.394		2^-_2	0.125		3^-_2	0.069		2^-_2	0.031		2^-_2	0.002	
2^-_3	0.617		2^-_3	0.180		3^-_3	0.044		2^-_3	0.037		2^-_3	0.001	
2^-_4	0.187		2^-_4	0.065		3^-_4	0.024		2^-_4	0.044		2^-_4	0.001	
2^-_5	0.502		2^-_5	0.091		3^-_5	0.010		2^-_5	0.011		2^-_5	0.001	
3^-_1	0.185	0.56[d]	3^-_1	0.040		5^-_1	0.096	0.90[d]	3^-_1	0.009		3^-_1	0.017	
3^-_2	0.089		3^-_2	0.124		5^-_2	0.060		3^-_2	0.025		3^-_2	0.006	
3^-_3	0.100		3^-_3	0.000		5^-_3	0.045		3^-_3	0.024		3^-_3	0.009	
3^-_4	0.127		3^-_4	0.103		5^-_4	0.032		3^-_4	0.001		3^-_4	0.006	
3^-_5	0.088		3^-_5	0.018		5^-_5	0.019		3^-_5	0.060		3^-_5	0.023	
4^-_1	0.379		4^-_1	0.283					4^-_1	0.023		4^-_1	0.005	
4^-_2	0.590		4^-_2	0.124					4^-_2	0.030		4^-_2	0.009	
4^-_3	0.180		4^-_3	0.177					4^-_3	0.036		4^-_3	0.007	
4^-_4	0.484		4^-_4	0.064					4^-_4	0.042		4^-_4	0.007	
4^-_5	0.127		4^-_5	0.089					4^-_5	0.0002		4^-_5	0.001	
5^-_1	0.180	0.39[d]	5^-_1	0.101	0.09[c]				5^-_1	0.019		5^-_1	0.020	
5^-_2	0.010		5^-_2	0.115					5^-_2	0.012		5^-_2	0.002	
5^-_3	0.110		5^-_3	0.002					5^-_3	0.043		5^-_3	0.010	
5^-_4	0.145		5^-_4	0.062					5^-_4	0.005		5^-_4	0.010	
5^-_5	0.063		5^-_5	0.045					5^-_5	0.045		5^-_5	0.011	
6^-_1	0.352		6^-_1	0.280	0.27[e], 0.16[f], 0.05[f]				6^-_1	0.021		6^-_1	0.011	
6^-_2	0.166		6^-_2	0.121					6^-_2	0.030		6^-_2	0.016	
6^-_3	0.438		6^-_3	0.170					6^-_3	0.031		6^-_3	0.013	
6^-_4	0.122		6^-_4	0.062					6^-_4	0.039		6^-_4	0.013	
6^-_5	0.276		6^-_5	0.086					6^-_5	0.001		6^-_5	0.002	

allowing mixing. The overall agreement with experiment is quite satisfactory, showing that the SACM is able to describe complicated structures of cluster systems in the *sd* shell.

The spectroscopic factors of the systems were also calculated and listed for later use in experimental deduction of fusion cross sections. In Ref. [31], it was shown that the SU(3) spectroscopic factors are reproduced extremely well for core+α systems. Here, we presented results of these factors near, but not in, the SU(3) limit.

ACKNOWLEDGMENTS

We gratefully acknowledge financial help from DGAPA-PAPIIT (Grant No. IN103212), from the National Research Council of Mexico (CONACyT), OTKA (Grant No. K72357), and from the MTA-CONACyT joint project. P.R.F. acknowledges travel funds from the Dipartimento di Fisica e Astronomia dell'Università di Padova, PRIN research project 2009TWL3MX. M.J.E.'s work is supported by Grant No. 17901 of CONACYT project CB2010/155633 and by Grant No. F2-FA-F177 of Uzbekistan Academy of Sciences.

APPENDIX A

Here, we present the formulas needed for the calculation of the matrix elements of the Hamiltonian, given in Eqs. (2) and (3). We start by considering only the nondiagonal interaction related to the SO(4) Hamiltonian. We use the formulas of Ref. [26], as listed in its Appendix. The triply reduced matrix elements of the bilinear products of creation and annihilation operators of the relative quanta are given by

$$\begin{aligned}\langle (n'_\pi,0)|||[\boldsymbol{\pi}^\dagger\otimes\boldsymbol{\pi}^\dagger]^{(2,0)}|||(n_\pi,0)\rangle &= \sqrt{n'_\pi(n'_\pi-1)}\,\delta_{n'_\pi,n_\pi+2}\\ \langle (n'_\pi,0)|||[\boldsymbol{\pi}\otimes\boldsymbol{\pi}]^{(0,2)}|||(n_\pi,0)\rangle &= \sqrt{(n'_\pi+3)(n'_\pi+4)}\,\delta_{n'_\pi,n_\pi-2}.\end{aligned} \tag{A1}$$

The triply reduced matrix elements of a pair of boson creation operators is given by

$$\langle \rho'_C(\lambda'_C,\mu'_C),(n'_\pi,0),(\lambda',\mu')|||[\boldsymbol{\pi}^\dagger\otimes\boldsymbol{\pi}^\dagger]^{(2,0)}|||\rho_C(\lambda_C,\mu_C),(n_\pi,0),(\lambda,\mu)\rangle_1$$
$$=\begin{Bmatrix}(\lambda_C,\mu_C) & (0,0) & (\lambda'_C,\mu'_C) & 1\\ (n_\pi,0) & (2,0) & (n'_\pi,0) & 1\\ (\lambda,\mu) & (2,0) & (\lambda',\mu') & 1\\ 1 & 1 & 1 & \end{Bmatrix}\langle (n'_\pi,0)|||[\boldsymbol{\pi}^\dagger\otimes\boldsymbol{\pi}^\dagger]^{(2,0)}|||(n_\pi,0)\rangle_1\delta_{(\lambda'_C,\mu'_C),(\lambda_C,\mu_C)}\delta_{\rho'_C,\rho_C} \tag{A2}$$

and a similar relation holds for the two annihilation operators. The symbol { } stands for the 9-(λ,μ) symbol. Please note that the total number of bosons (N) is conserved; thus, the number of σ bosons is determined by n_π, so our shorthand notation for the basis states is complete.

The next type of interaction is the product of two creation and two annihilation operators, i.e.,

$$\langle \rho'_C(\lambda'_C,\mu'_C),(n'_\pi,0),(\lambda',\mu')|||[[\boldsymbol{\pi}^\dagger\otimes\boldsymbol{\pi}^\dagger]^{(2,0)}\otimes[\boldsymbol{\pi}\otimes\boldsymbol{\pi}]^{(0,2)}]^{(\lambda_0,\lambda_0)}|||\rho_C(\lambda_C,\mu_C),(n_\pi,0),(\lambda,\mu)\rangle_1$$
$$=\begin{Bmatrix}(\lambda_C,\mu_C) & (0,0) & (\lambda'_C,\mu'_C) & 1\\ (n_\pi,0) & (\lambda_0,\lambda_0) & (n'_\pi,0) & 1\\ (\lambda,\mu) & (\lambda_0,\lambda_0) & (\lambda',\mu') & 1\\ 1 & 1 & 1 & \end{Bmatrix}\delta_{(\lambda'_C,\mu'_C),(\lambda_C,\mu_C)}\delta_{\rho'_C,\rho_C}\delta_{n'_\pi,n_\pi}$$
$$\times\langle (n'_\pi,0)|||[\boldsymbol{\pi}^\dagger\otimes\boldsymbol{\pi}^\dagger]^{(2,0)}|||(n_\pi-2,0)\rangle_1\langle (n_\pi-2,0)|||[\boldsymbol{\pi}\otimes\boldsymbol{\pi}]^{(0,2)}|||(n_\pi,0)\rangle_1$$
$$\times U[(n_\pi,0)(0,2)(n'_\pi,0)(20);(n_\pi-2,0)11(\lambda_0,\lambda_0)11], \tag{A3}$$

with $\lambda_0=0,1,2$ and $U[\cdots]$ being the SU(3) Racah coefficient [26]. Here, only irreps of the form (λ_0,λ_0) appear and any others can be deduced as follows: A creation operator of π bosons transforms as $(1,0)$ and a product of two as $(2,0)$, because this product is symmetric. For the annihilation operators the argument is the same, except that one annihilation operator transforms as $(0,1)$ and two as $(0,2)$. A product of two creation and two annihilation operators thus can be coupled to $(2,0)\otimes(0,2)=(2,2)+(1,1)+(0,0)$, i.e., to irreps with $\mu_0=\lambda_0$. The Kronecker δ function for the n_π bosons enters because the operator in consideration does not change this number.

In the Hamiltonian, only those products of two creation and two annihilation operators appear, which are coupled to zero angular momentum. Their relations to the SU(3) tensor products are

$$(\boldsymbol{\pi}^\dagger\cdot\boldsymbol{\pi}^\dagger)=\sqrt{3}\langle(1,0)11,(1,0)11||(2,0)10\rangle_1[\boldsymbol{\pi}^\dagger\otimes\boldsymbol{\pi}^\dagger]^{(2,0)}_{100}$$
$$(\boldsymbol{\pi}\cdot\boldsymbol{\pi})=\sqrt{3}\langle(0,1)11,(0,1)11||(0,2)10\rangle_1[\boldsymbol{\pi}\otimes\boldsymbol{\pi}]^{(0,2)}_{100} \tag{A4}$$

and

$$(\boldsymbol{\pi}^\dagger\cdot\boldsymbol{\pi}^\dagger)(\boldsymbol{\pi}\cdot\boldsymbol{\pi})=3\sum_{\lambda_0}\langle(1,0)11,(1,0)11||(2,0)10\rangle_1\langle(0,1)11,(0,1)11||(0,2)10\rangle_1$$
$$\times\langle(2,0)10,(0,2)10||(\lambda_0,\lambda_0)10\rangle_1[[\boldsymbol{\pi}^\dagger\otimes\boldsymbol{\pi}^\dagger]^{(2,0)}\otimes[\boldsymbol{\pi}\otimes\boldsymbol{\pi}]^{(0,2)}]^{(\lambda_0,\lambda_0)}_{100}, \tag{A5}$$

where the subindex in the last line refers to the multiplicity $\kappa=1$, angular momentum $L=0$, and its projection $m=0$, respectively.

The matrix elements of the $\sigma^\dagger$ and σ operators are

$$\begin{aligned}\langle n'_\sigma|\boldsymbol{\sigma}^\dagger|n_\sigma\rangle &= \delta_{n'_\sigma n_\sigma+1}\sqrt{n_\sigma+1}\\ \langle n'_\sigma|\boldsymbol{\sigma}|n_\sigma\rangle &= \delta_{n'_\sigma n_\sigma-1}\sqrt{n_\sigma}\\ \langle n'_\sigma|\boldsymbol{\sigma}^\dagger\boldsymbol{\sigma}|n_\sigma\rangle &= \delta_{n'_\sigma n_\sigma}n_\sigma\\ \langle n'_\sigma|(\boldsymbol{\sigma}^\dagger)^2|n_\sigma\rangle &= \delta_{n'_\sigma n_\sigma+2}\sqrt{(n_\sigma+1)(n_\sigma+2)}\\ \langle n'_\sigma|(\boldsymbol{\sigma})^2|n_\sigma\rangle &= \delta_{n'_\sigma n_\sigma-2}\sqrt{n_\sigma(n_\sigma-1)},\end{aligned} \tag{A6}$$

where we denoted the basis states by the $n_\sigma=N-n_\pi$ quantum number.

For the quadrupole and angular-momentum interaction we have, in general,

$$\boldsymbol{Q}\cdot\boldsymbol{Q}=4\boldsymbol{C}_2(\mathrm{SU}(3))-3\boldsymbol{L}^2, \tag{A7}$$

with

$$\boldsymbol{L}^2=\sqrt{\frac{15}{8}}[\boldsymbol{C}^{(1,1)}\otimes\boldsymbol{C}^{(1,1)}]^{(2,2)}_{100}+\sqrt{\frac{9}{8}}[\boldsymbol{C}^{(1,1)}\otimes\boldsymbol{C}^{(1,1)}]^{(0,0)}_{100}, \tag{A8}$$

where $\boldsymbol{C}^{(1,1)}$ are the generators of any of the SU(3) groups. In order to evaluate the matrix elements of the quadrupole-quadrupole interaction, the following triply reduced matrix elements are needed,

$$\begin{aligned}&\langle(\lambda_1',\mu_1'),(\lambda_2',\mu_2');\rho_C'(\lambda_C',\mu_C'),(n_\pi',0);(\lambda',\mu')\|\left[\boldsymbol{C}_i^{(1,1)}\otimes\boldsymbol{C}_i^{(1,1)}\right]^{(0,0)}\|(\lambda_1,\mu_1),(\lambda_2,\mu_2);\rho_C(\lambda_C,\mu_C),(n_\pi,0);(\lambda,\mu)\rangle_1\\&\quad=\delta_{n_\pi,n_\pi'}\delta_{(\lambda_C,\mu_C),(\lambda_C',\mu_C')}\delta_{(\lambda,\mu),(\lambda',\mu')}\delta_{\rho_C',\rho_C}\delta_{(\lambda_1,\mu_1),(\lambda_1',\mu_1')}\delta_{(\lambda_2,\mu_2),(\lambda_2',\mu_2')}\langle(\lambda_i,\mu_i)\|\left[\boldsymbol{C}_i^{(1,1)}\otimes\boldsymbol{C}_i^{(1,1)}\right]^{(0,0)}\|(\lambda_i,\mu_i)\rangle_{\rho_i=1},\end{aligned}\tag{A9}$$

where

$$\langle(\lambda_i,\mu_i)\|\left[\boldsymbol{C}_i^{(1,1)}\otimes\boldsymbol{C}_i^{(1,1)}\right]^{(0,0)}\|(\lambda_i,\mu_i)\rangle_{\rho_i=1}=\frac{\sqrt{2}}{3}\left(\lambda_i^2+\mu_i^2+\lambda_i\mu_i+3\lambda_i+3\mu_i\right).\tag{A10}$$

Next we need to evaluate the triply reduced matrix element,

$$\langle(\lambda_1',\mu_1'),(\lambda_2',\mu_2');\rho_C'(\lambda_C',\mu_C'),(n_\pi',0);(\lambda',\mu')\|\left[\boldsymbol{C}_i^{(1,1)}\otimes\boldsymbol{C}_i^{(1,1)}\right]^{(2,2)}\|(\lambda_1,\mu_1),(\lambda_2,\mu_2);\rho_C(\lambda_C,\mu_C),(n_\pi,0);(\lambda,\mu)\rangle_\rho.\tag{A11}$$

The evaluation of this term depends on the value taken by i ($i=1,2,C,R$). In the $i=1$ case,

$$\begin{aligned}&\langle(\lambda_1',\mu_1'),(\lambda_2',\mu_2');\rho_C'(\lambda_C',\mu_C'),(n_\pi',0);(\lambda',\mu')\|\left[\boldsymbol{C}_1^{(1,1)}\otimes\boldsymbol{C}_1^{(1,1)}\right]^{(2,2)}\|(\lambda_1,\mu_1),(\lambda_2,\mu_2);\rho_C(\lambda_C,\mu_C),(n_\pi,0);(\lambda,\mu)\rangle_\rho\\&\quad=\delta_{n_\pi,n_\pi'}\delta_{(\lambda_2,\mu_2),(\lambda_2',\mu_2')}\sum_{\tilde\rho_C}\begin{Bmatrix}(\lambda_C,\mu_C)&(2,2)&(\lambda_C',\mu_C')&\tilde\rho_C\\(n_\pi,0)&(0,0)&(n_\pi,0)&1\\(\lambda,\mu)&(2,2)&(\lambda',\mu')&\rho\\1&1&1&\end{Bmatrix}\sum_{\tilde\rho}\begin{Bmatrix}(\lambda_1,\mu_1)&(2,2)&(\lambda_1',\mu_1')&\tilde\rho\\(\lambda_2,\mu_2)&(0,0)&(\lambda_2,\mu_2)&1\\(\lambda_C,\mu_C)&(2,2)&(\lambda_C',\mu_C')&\tilde\rho_C\\\rho_C&1&\rho_C'&\end{Bmatrix}\\&\quad\times\langle(\lambda_1',\mu_1')\|\left[\boldsymbol{C}_1^{(1,1)}\otimes\boldsymbol{C}_1^{(1,1)}\right]^{(2,2)}\|(\lambda_1,\mu_1)\rangle_{\tilde\rho},\end{aligned}\tag{A12}$$

where

$$\begin{aligned}&\langle(\lambda_1',\mu_1')\|\left[\boldsymbol{C}_1^{(1,1)}\otimes\boldsymbol{C}_1^{(1,1)}\right]^{(2,2)}\|(\lambda_1,\mu_1)\rangle_{\tilde\rho}\\&\quad=\sum_{(\lambda_1'',\mu_1'')\rho^\otimes\rho^*}\langle(\lambda_1',\mu_1')\|\boldsymbol{C}_1^{(1,1)}\|(\lambda_1'',\mu_1'')\rangle_{\rho^\otimes}\langle(\lambda_1'',\mu_1'')\|\boldsymbol{C}_1^{(1,1)}\|(\lambda_1,\mu_1)\rangle_{\rho^*}\\&\qquad\times\sum_{\rho_k}\Phi_{1\rho_k}[(1,1),(1,1),(2,2)]U[(\lambda_1,\mu_1)(1,1)(\lambda_1',\mu_1')(1,1);(\lambda_1'',\mu_1'')\rho^*\rho^\otimes(2,2)\rho_k\tilde\rho]\\&\quad=\delta_{(\lambda_1,\mu_1),(\lambda_1',\mu_1')}\left[\langle(\lambda_1,\mu_1)\|\boldsymbol{C}_1^{(1,1)}\|(\lambda_1,\mu_1)\rangle_1\right]^2U\left[(\lambda_1,\mu_1)(1,1)(\lambda_1,\mu_1)(1,1);(\lambda_1,\mu_1)11(2,2)1\tilde\rho\right],\end{aligned}\tag{A13}$$

with

$$\langle(\lambda_j,\mu_j)\|C_j^{(1,1)}\|(\lambda_j,\mu_j)\rangle_{\rho_j=1}=(-1)^\phi\left(\frac{4}{3}\left(\lambda_j^2+\mu_j^2+\lambda_j\mu_j+3\lambda_j+3\mu_j\right)\right)^{1/2},\tag{A14}$$

where $\phi=0$ holds if $\mu_j=0$, and $\phi=1$ otherwise. This is in accordance with Ref. [26].

Now for $i=2$, we obtain

$$\begin{aligned}&\langle(\lambda_1',\mu_1'),(\lambda_2',\mu_2');\rho_C'(\lambda_C',\mu_C'),(n_\pi',0);(\lambda',\mu')\|\left[\boldsymbol{C}_2^{(1,1)}\otimes\boldsymbol{C}_2^{(1,1)}\right]^{(2,2)}\|(\lambda_1,\mu_1),(\lambda_2,\mu_2);\rho_C(\lambda_C,\mu_C),(n_\pi,0);(\lambda,\mu)\rangle_\rho\\&\quad=\delta_{n_\pi,n_\pi'}\delta_{(\lambda_1,\mu_1),(\lambda_1',\mu_1')}\sum_{\tilde\rho_C}\begin{Bmatrix}(\lambda_C,\mu_C)&(2,2)&(\lambda_C',\mu_C')&\tilde\rho_C\\(n_\pi,0)&(0,0)&(n_\pi,0)&1\\(\lambda,\mu)&(2,2)&(\lambda',\mu')&\rho\\1&1&1&\end{Bmatrix}\sum_{\tilde\rho}\begin{Bmatrix}(\lambda_1,\mu_1)&(0,0)&(\lambda_1,\mu_1)&1\\(\lambda_2,\mu_2)&(2,2)&(\lambda_2',\mu_2')&\tilde\rho\\(\lambda_C,\mu_C)&(2,2)&(\lambda_C',\mu_C')&\bar\rho_C\\\rho_C&1&\rho_C'&\end{Bmatrix}\\&\quad\times\langle(\lambda_2',\mu_2')\|\left[\boldsymbol{C}_2^{(1,1)}\otimes\boldsymbol{C}_2^{(1,1)}\right]^{(2,2)}\|(\lambda_2,\mu_2)\rangle_{\tilde\rho},\end{aligned}\tag{A15}$$

where

$$\begin{aligned}
&\langle(\lambda_2',\mu_2')||\big[\boldsymbol{C}_2^{(1,1)}\otimes\boldsymbol{C}_2^{(1,1)}\big]^{(2,2)}||(\lambda_2,\mu_2)\rangle_{\tilde\rho}\\
&\quad=\sum_{(\lambda_2'',\mu_2'')\rho^{\otimes}\rho^*}\langle(\lambda_2',\mu_2')||\boldsymbol{C}_2^{(1,1)}||(\lambda_2'',\mu_2'')\rangle_{\rho^{\otimes}}\langle(\lambda_2'',\mu_2'')||\boldsymbol{C}_2^{(1,1)}||(\lambda_2,\mu_2)\rangle_{\rho^*}\\
&\qquad\times\sum_{\rho_k}\Phi_{1\rho_k}[(1,1),(1,1),(2,2)]U[(\lambda_2,\mu_2)(1,1)(\lambda_2',\mu_2')(1,1);(\lambda_2'',\mu_2'')\rho^*\rho^{\otimes}(2,2)\rho_k\tilde\rho]\\
&\quad=\delta_{(\lambda_2,\mu_2),(\lambda_2',\mu_2')}\big[\langle(\lambda_2,\mu_2)||\boldsymbol{C}_2^{(1,1)}||(\lambda_2,\mu_2)\rangle_1\big]^2U[(\lambda_2,\mu_2)(1,1)(\lambda_2,\mu_2)(1,1);(\lambda_2,\mu_2)11(2,2)1\tilde\rho].
\end{aligned}\tag{A16}$$

Similarly, we can obtain for the case $i=R$ the next result,

$$\begin{aligned}
&\langle(\lambda_1',\mu_1'),(\lambda_2',\mu_2');\rho_C'(\lambda_C',\mu_C'),(n_\pi',0);(\lambda',\mu')||\big[\boldsymbol{C}_R^{(1,1)}\otimes\boldsymbol{C}_R^{(1,1)}\big]^{(2,2)}||(\lambda_1,\mu_1),(\lambda_2,\mu_2);\rho_C(\lambda_C,\mu_C),(n_\pi,0);(\lambda,\mu)\rangle_\rho\\
&=\delta_{(\lambda_1,\mu_1),(\lambda_1',\mu_1')}\delta_{(\lambda_2,\mu_2),(\lambda_2',\mu_2')}\delta_{(\lambda_C,\mu_C),(\lambda_C',\mu_C')}\begin{Bmatrix}(\lambda_C,\mu_C)&(0,0)&(\lambda_C,\mu_C)&1\\(n_\pi,0)&(2,2)&(n_\pi',0)&1\\(\lambda,\mu)&(2,2)&(\lambda',\mu')&\rho\\1&1&1&\end{Bmatrix}\langle(n_\pi',0)||\big[\boldsymbol{C}_R^{(1,1)}\otimes\boldsymbol{C}_R^{(1,1)}\big]^{(2,2)}||(n_\pi,0)\rangle_1,
\end{aligned}\tag{A17}$$

where

$$\begin{aligned}
&\langle(n_\pi',0)||\big[\boldsymbol{C}_R^{(1,1)}\otimes\boldsymbol{C}_R^{(1,1)}\big]^{(2,2)}||(n_\pi,0)\rangle_1\\
&\quad=\sum_{n_\pi''\rho^{\otimes}\rho^*}\langle(n_\pi',0)||\boldsymbol{C}_R^{(1,1)}||(n_\pi'',0)\rangle_{\rho^{\otimes}}\langle(n_\pi'',0)||\boldsymbol{C}_R^{(1,1)}||(n_\pi,0)\rangle_{\rho^*}\\
&\qquad\times\sum_{\rho_k}\Phi_{1\rho_k}[(1,1),(1,1),(2,2)]U[(n_\pi,0)(1,1)(n_\pi',0)(1,1);(n_\pi'',0)\rho^*\rho^{\otimes}(2,2)\rho_k1]\\
&\quad=\delta_{n_\pi,n_\pi'}\big[\langle(n_\pi,0)||\boldsymbol{C}_R^{(1,1)}||(n_\pi,0)\rangle_1\big]^2U[(n_\pi,0)(1,1)(n_\pi,0)(1,1);(n_\pi,0)11(2,2)11].
\end{aligned}\tag{A18}$$

Finally, when $i=C$, we have

$$\begin{aligned}
&\langle(\lambda_1',\mu_1'),(\lambda_2',\mu_2');\rho_C'(\lambda_C',\mu_C'),(n_\pi',0);(\lambda',\mu')||\big[\boldsymbol{C}_C^{(1,1)}\otimes\boldsymbol{C}_C^{(1,1)}\big]^{(2,2)}||(\lambda_1,\mu_1),(\lambda_2,\mu_2);\rho_C(\lambda_C,\mu_C),(n_\pi,0);(\lambda,\mu)\rangle_\rho\\
&=\delta_{n_\pi,n_\pi'}\sum_{\tilde\rho_C}\begin{Bmatrix}(\lambda_C,\mu_C)&(2,2)&(\lambda_C',\mu_C')&\tilde\rho_C\\(n_\pi,0)&(0,0)&(n_\pi,0)&1\\(\lambda,\mu)&(2,2)&(\lambda',\mu')&\rho\\1&1&1&\end{Bmatrix}\langle(\lambda_C',\mu_C')||\big[\boldsymbol{C}_C^{(1,1)}\otimes\boldsymbol{C}_C^{(1,1)}\big]^{(2,2)}||(\lambda_C,\mu_C)\rangle_{\tilde\rho_C},
\end{aligned}\tag{A19}$$

where

$$\begin{aligned}
&\langle(\lambda_C',\mu_C')||\big[\boldsymbol{C}_C^{(1,1)}\otimes\boldsymbol{C}_C^{(1,1)}\big]^{(2,2)}||(\lambda_C,\mu_C)\rangle_{\tilde\rho_C}\\
&\quad=\sum_{(\lambda_C'',\mu_C'')\rho^{\otimes}\rho^*}\langle(\lambda_C',\mu_C')||\boldsymbol{C}_R^{(1,1)}||(\lambda_C'',\mu_C'')\rangle_{\rho^{\otimes}}\langle(\lambda_C'',\mu_C'')||\boldsymbol{C}_R^{(1,1)}||(\lambda_C,\mu_C)\rangle_{\rho^*}\\
&\qquad\times\sum_{\rho_k}\Phi_{1\rho_k}[(1,1),(1,1),(2,2)]U[(\lambda_C,\mu_C)(1,1)(\lambda_C',\mu_C')(1,1);(\lambda_C'',\mu_C'')\rho^*\rho^{\otimes}(2,2)\rho_k\tilde\rho_C]\\
&\quad=\delta_{(\lambda_C,\mu_C),(\lambda_C',\mu_C')}\big[\langle(\lambda_C,\mu_C)||\boldsymbol{C}_C^{(1,1)}||(\lambda_C,\mu_C)\rangle_1\big]^2U[(\lambda_C,\mu_C)(1,1)(\lambda_C,\mu_C)(1,1);(\lambda_C,\mu_C)11(2,2)1\tilde\rho_C].
\end{aligned}\tag{A20}$$

Next we need to evaluate the following interaction terms which appear in the Hamiltonian (2) and (3),

$$\boldsymbol{Q}_i\cdot\boldsymbol{Q}_j=-3\sqrt{\frac{15}{8}}\big[\boldsymbol{C}_i^{(1,1)}\otimes\boldsymbol{C}_j^{(1,1)}\big]_{100}^{(2,2)}+5\sqrt{\frac{9}{8}}\big[\boldsymbol{C}_i^{(1,1)}\otimes\boldsymbol{C}_j^{(1,1)}\big]_{100}^{(0,0)},\tag{A21}$$

with $i = 1,\ 2,$ and $j = R$, additionally

$$\boldsymbol{L}_i \cdot \boldsymbol{L}_j = \sqrt{\frac{15}{8}}\left[\boldsymbol{C}_i^{(1,1)} \otimes \boldsymbol{C}_j^{(1,1)}\right]_{100}^{(2,2)} + \sqrt{\frac{9}{8}}\left[\boldsymbol{C}_i^{(1,1)} \otimes \boldsymbol{C}_j^{(1,1)}\right]_{100}^{(0,0)}, \tag{A22}$$

where $\boldsymbol{C}_i^{(1,1)}$ are the generators of the $\mathrm{SU}_i(3)$ group. For the case of $i = 1$ we obtain

$$\begin{aligned}
&\langle (\lambda_1', \mu_1'), (\lambda_2', \mu_2'); \rho_C'(\lambda_C', \mu_C'), (n_\pi', 0); (\lambda', \mu') || \left[\boldsymbol{C}_1^{(1,1)} \otimes \boldsymbol{C}_R^{(1,1)}\right]^{(0,0)} || |(\lambda_1, \mu_1), (\lambda_2, \mu_2); \rho_C(\lambda_C, \mu_C), (n_\pi, 0); (\lambda, \mu)\rangle_1 \\
&= \delta_{n_\pi, n_\pi'} \delta_{(\lambda,\mu),(\lambda',\mu')} \delta_{(\lambda_1,\mu_1),(\lambda_1',\mu_1')} \delta_{(\lambda_2,\mu_2),(\lambda_2',\mu_2')} \sum_{\tilde{\rho}_C} \begin{Bmatrix} (\lambda_C, \mu_C) & (1,1) & (\lambda_C', \mu_C') & \tilde{\rho}_C \\ (n_\pi, 0) & (1,1) & (n_\pi, 0) & 1 \\ (\lambda, \mu) & (0,0) & (\lambda, \mu) & 1 \\ 1 & 1 & 1 & \end{Bmatrix} \begin{Bmatrix} (\lambda_1, \mu_1) & (1,1) & (\lambda_1, \mu_1) & 1 \\ (\lambda_2, \mu_2) & (0,0) & (\lambda_2, \mu_2) & 1 \\ (\lambda_C, \mu_C) & (1,1) & (\lambda_C', \mu_C') & \tilde{\rho}_C \\ \rho_C & 1 & \rho_C' & \end{Bmatrix} \\
&\quad \times \langle (\lambda_1, \mu_1) || \boldsymbol{C}_1^{(1,1)} || |(\lambda_1, \mu_1)\rangle (n_\pi, 0) || \boldsymbol{C}_R^{(1,1)} || |(n_\pi, 0)\rangle
\end{aligned} \tag{A23}$$

and

$$\begin{aligned}
&\langle (\lambda_1', \mu_1'), (\lambda_2', \mu_2'); \rho_C'(\lambda_C', \mu_C'), (n_\pi', 0); (\lambda', \mu') || \left[\boldsymbol{C}_1^{(1,1)} \otimes \boldsymbol{C}_R^{(1,1)}\right]^{(2,2)} || |(\lambda_1, \mu_1), (\lambda_2, \mu_2); \rho_C(\lambda_C, \mu_C), (n_\pi, 0); (\lambda, \mu)\rangle_\rho \\
&= \delta_{n_\pi, n_\pi'} \delta_{(\lambda_1,\mu_1),(\lambda_1',\mu_1')} \delta_{(\lambda_2,\mu_2),(\lambda_2',\mu_2')} \sum_{\tilde{\rho}_C} \begin{Bmatrix} (\lambda_C, \mu_C) & (1,1) & (\lambda_C', \mu_C') & \tilde{\rho}_C \\ (n_\pi, 0) & (1,1) & (n_\pi, 0) & 1 \\ (\lambda, \mu) & (2,2) & (\lambda', \mu') & \rho \\ 1 & 1 & 1 & \end{Bmatrix} \begin{Bmatrix} (\lambda_1, \mu_1) & (1,1) & (\lambda_1, \mu_1) & 1 \\ (\lambda_2, \mu_2) & (0,0) & (\lambda_2, \mu_2) & 1 \\ (\lambda_C, \mu_C) & (1,1) & (\lambda_C', \mu_C') & \tilde{\rho}_C \\ \rho_C & 1 & \rho_C' & \end{Bmatrix} \\
&\quad \times \langle (\lambda_1, \mu_1) || \boldsymbol{C}_1^{(1,1)} || |(\lambda_1, \mu_1)\rangle (n_\pi, 0) || \boldsymbol{C}_R^{(1,1)} || |(n_\pi, 0)\rangle,
\end{aligned} \tag{A24}$$

similar formulas can be obtained for the second cluster ($i = 2$).

APPENDIX B

1. Matrix elements for the electric quadrupole transitions

The relations of the quadrupole operator to the $C_{2m}^{(1,1)}$ generators of the SU(3) group, expressed in terms of SU(3)-coupled π-boson creation and annihilation operators [26], are

$$\boldsymbol{Q}_{i\,m}^{(2)} = \frac{1}{\sqrt{3}} C_{2m}^{(1,1)} = \sqrt{\frac{2}{3}} [\boldsymbol{\pi}^\dagger \otimes \boldsymbol{\pi}]_{2m}^{(1,1)}, \tag{B1}$$

where $i = 1,\ 2$ and, for the relative motion, $\boldsymbol{Q}_{R\,m}^{(2)}$ is given by

$$\boldsymbol{Q}_{R\,m}^{(2)} = \sqrt{3} C_{2m}^{(1,1)} = \sqrt{6} [\boldsymbol{\pi}^\dagger \otimes \boldsymbol{\pi}]_{2m}^{(1,1)}. \tag{B2}$$

With the standard SU(3) coupling and recoupling techniques the following matrix elements are obtained in terms of SU(3) isoscalar factors and $9(\lambda, \mu)$ symbols.

$$\begin{aligned}
&\left\langle (\lambda_1', \mu_1'), (\lambda_2', \mu_2'); \rho_C'(\lambda_C', \mu_C'), (n_\pi', 0); (\lambda', \mu') K' L' \middle|\middle| Q_1^{(2)12} \middle|\middle| (\lambda_1, \mu_1), (\lambda_2, \mu_2); \rho_C(\lambda_C, \mu_C), (n_\pi, 0); (\lambda, \mu) K L \right\rangle \\
&= \frac{1}{\sqrt{3}} \delta_{n_\pi, n_\pi'} \delta_{(\lambda_1,\mu_1),(\lambda_1',\mu_1')} \delta_{(\lambda_2,\mu_2),(\lambda_2',\mu_2')} \langle (\lambda_1, \mu_1) || C_1^{(1,1)} || |(\lambda_1, \mu_1)\rangle_{\rho_1 = 1} \sum_{\tilde{\rho}} \langle (\lambda, \mu) K L, (1,1) 12 || (\lambda', \mu') K' L' \rangle_{\tilde{\rho}} \\
&\quad \times \sum_{\tilde{\rho}_C} \begin{Bmatrix} (\lambda_C, \mu_C) & (1,1) & (\lambda_C', \mu_C') & \tilde{\rho}_C \\ (n_\pi, 0) & (0,0) & (n_\pi, 0) & 1 \\ (\lambda, \mu) & (1,1) & (\lambda', \mu') & \tilde{\rho} \\ 1 & 1 & 1 & \end{Bmatrix} \begin{Bmatrix} (\lambda_1, \mu_1) & (1,1) & (\lambda_1, \mu_1) & 1 \\ (\lambda_2, \mu_2) & (0,0) & (\lambda_2, \mu_2) & 1 \\ (\lambda_C, \mu_C) & (1,1) & (\lambda_C', \mu_C') & \tilde{\rho}_C \\ \rho_C & 1 & \rho_C' & \end{Bmatrix}.
\end{aligned} \tag{B3}$$

Note that in several places the multiplicities of the SU(3) couplings turn out to be 1, partly due to the fact that the multiplication involved SU(3) irreps of the type $(\lambda, 0)$ or $(0, \mu)$ and partly because the group generator appeared in the product.

A similar formula results for the quadrupole momentum operator of the other cluster,

$$\begin{aligned}
&\left\langle (\lambda_1', \mu_1'), (\lambda_2', \mu_2'); \rho_C'(\lambda_C', \mu_C'), (n_\pi', 0); (\lambda', \mu') K' L' \middle|\middle| Q_2^{(2)12} \middle|\middle| (\lambda_1, \mu_1), (\lambda_2, \mu_2); \rho_C(\lambda_C, \mu_C), (n_\pi, 0); (\lambda, \mu) K L \right\rangle \\
&= \frac{1}{\sqrt{3}} \delta_{n_\pi, n_\pi'} \delta_{(\lambda_1,\mu_1),(\lambda_1',\mu_1')} \delta_{(\lambda_2,\mu_2),(\lambda_2',\mu_2')} \langle (\lambda_2, \mu_2) || \big| C_2^{(1,1)} \big| | (\lambda_2, \mu_2) \rangle_{\rho_2=1} \sum_{\tilde{\rho}} \langle (\lambda, \mu) K L, (1,1) 12 || (\lambda', \mu') K' L' \rangle_{\tilde{\rho}} \\
&\quad \times \sum_{\tilde{\rho}_C} \begin{Bmatrix} (\lambda_C, \mu_C) & (1,1) & (\lambda_C', \mu_C') & \tilde{\rho}_C \\ (n_\pi, 0) & (0,0) & (n_\pi, 0) & 1 \\ (\lambda, \mu) & (1,1) & (\lambda', \mu') & \tilde{\rho} \\ 1 & 1 & 1 & \end{Bmatrix} \begin{Bmatrix} (\lambda_1, \mu_1) & (0,0) & (\lambda_1, \mu_1) & 1 \\ (\lambda_2, \mu_2) & (1,1) & (\lambda_2, \mu_2) & 1 \\ (\lambda_C, \mu_C) & (1,1) & (\lambda_C', \mu_C') & \tilde{\rho}_C \\ \rho_C & 1 & \rho_C' & \end{Bmatrix}.
\end{aligned} \tag{B4}$$

Somewhat simpler formulas hold for the joint cluster (C) and relative (R) quadrupole momentum operators. Of these, the first is not independent, but rather it should be the sum of Eqs. (B3) and (B4), but we present it because it has a simpler form this way:

$$\begin{aligned}
&\left\langle (\lambda_1', \mu_1'), (\lambda_2', \mu_2'); \rho_C'(\lambda_C', \mu_C'), (n_\pi', 0); (\lambda', \mu') K' L' \middle|\middle| Q_C^{(2)12} \middle|\middle| (\lambda_1, \mu_1), (\lambda_2, \mu_2); \rho_C(\lambda_C, \mu_C), (n_\pi, 0); (\lambda, \mu) K L \right\rangle \\
&= \frac{1}{\sqrt{3}} \delta_{n_\pi, n_\pi'} \delta_{(\lambda_C,\mu_C),(\lambda_C',\mu_C')} \delta_{\rho_C', \rho_C} \langle (\lambda_C, \mu_C) || \big| C_C^{(1,1)} \big| | (\lambda_C, \mu_C) \rangle_{\tilde{\rho}_C=1} \\
&\quad \times \sum_{\tilde{\rho}} \langle (\lambda, \mu) K L, (1,1) 12 || (\lambda', \mu') K' L' \rangle_{\tilde{\rho}} \begin{Bmatrix} (\lambda_C, \mu_C) & (1,1) & (\lambda_C', \mu_C') & \tilde{\rho}_C = 1 \\ (n_\pi, 0) & (0,0) & (n_\pi', 0) & 1 \\ (\lambda, \mu) & (1,1) & (\lambda', \mu') & \tilde{\rho} \\ 1 & 1 & 1 & \end{Bmatrix}.
\end{aligned} \tag{B5}$$

Similarly, for the relative (R) quadrupole momentum operator, one obtains

$$\begin{aligned}
&\left\langle (\lambda_1', \mu_1'), (\lambda_2', \mu_2'); \rho_C'(\lambda_C', \mu_C'), (n_\pi', 0); (\lambda', \mu') K' L' \middle|\middle| Q_R^{(2)12} \middle|\middle| (\lambda_1, \mu_1), (\lambda_2, \mu_2); \rho_C(\lambda_C, \mu_C), (n_\pi, 0); (\lambda, \mu) K L \right\rangle \\
&= \sqrt{3} \delta_{n_\pi, n_\pi'} \delta_{(\lambda_C,\mu_C),(\lambda_C',\mu_C')} \delta_{\rho_C', \rho_C} \delta_{(\lambda_1,\mu_1),(\lambda_1',\mu_1')} \delta_{(\lambda_2,\mu_2),(\lambda_2',\mu_2')} \langle (n_\pi, 0) || \big| C_R^{(1,1)} \big| | (n_\pi, 0) \rangle_{\tilde{\rho}_R=1} \\
&\quad \times \sum_{\tilde{\rho}} \langle (\lambda, \mu) K L, (1,1) 12 || (\lambda', \mu') K' L' \rangle_{\tilde{\rho}} \begin{Bmatrix} (\lambda_C, \mu_C) & (0,0) & (\lambda_C, \mu_C) & 1 \\ (n_\pi, 0) & (1,1) & (n_\pi', 0) & \tilde{\rho}_R = 1 \\ (\lambda, \mu) & (1,1) & (\lambda', \mu') & \tilde{\rho} \\ 1 & 1 & 1 & \end{Bmatrix}.
\end{aligned} \tag{B6}$$

In all the above formulas the triply reduced matrix elements can be evaluated from the equation

$$\langle (\lambda_j, \mu_j) || \big| C_j^{(1,1)} \big| | (\lambda_j, \mu_j) \rangle_{\rho_j=1} = (-1)^\phi \left[\frac{4}{3} \left(\lambda_j^2 + \mu_j^2 + \lambda_j \mu_j + 3\lambda_j + 3\mu_j \right) \right]^{1/2}, \tag{B7}$$

where $j = 1, 2, C$ or R, and $\phi = 0$ holds if $\mu_j = 0$ and $\phi = 1$ otherwise. This choice is in accordance with the convention adopted by Escher and Draayer [26].

2. Matrix elements for the electric dipole transitions

The electric dipole transition operator given by

$$\left\langle e_R^{(1)} \boldsymbol{D}_{R,m}^{(1)} \right\rangle = e_R^{(1)} \langle \pi_m^\dagger s + s^\dagger \pi_m \rangle, \tag{B8}$$

and is the sum of two $\mathrm{SU}_R(3)$ tensors, $\pi_m^\dagger$ with $(\lambda_R, \mu_R) = (1, 0)$ and π_m with $(\lambda_R, \mu_R) = (0, 1)$. The first increases the number of π bosons by one unit, while the latter decreases it by one unit. Considering the general form of the dipole transition operator $D^{(\lambda_R, \mu_R)}$, and having in mind that this operator acts only on the radial part of the wave function, its matrix element is

given by

$$\left\langle (\lambda_1', \mu_1'), (\lambda_2', \mu_2'); \rho_C'(\lambda_C', \mu_C'), (n_\pi', 0); (\lambda', \mu')K'L' \middle|\middle| D_R^{(\lambda_R,\mu_R)01} \middle|\middle| (\lambda_1, \mu_1), (\lambda_2, \mu_2); \rho_C(\lambda_C, \mu_C), (n_\pi, 0); (\lambda, \mu)KL \right\rangle$$
$$= \delta_{(\lambda_C,\mu_C),(\lambda_C',\mu_C')}\delta_{\rho_C',\rho_C}\delta_{(\lambda_1,\mu_1),(\lambda_1',\mu_1')}\delta_{(\lambda_2,\mu_2),(\lambda_2',\mu_2')}\langle (n_\pi', 0)|\big|\big| D_R^{(\lambda_R,\mu_R)} \big|\big|\big| (n_\pi, 0)\rangle_{\tilde{\rho}_R=1} \sum_{\tilde{\rho}} \langle (\lambda, \mu)KL, (\lambda_R, \mu_R)01||(\lambda', \mu')K'L'\rangle_{\tilde{\rho}}$$
$$\times \begin{Bmatrix} (\lambda_C, \mu_C) & (0, 0) & (\lambda_C, \mu_C) & 1 \\ (n_\pi, 0) & (\lambda_R, \mu_R) & (n_\pi', 0) & \tilde{\rho}_R = 1 \\ (\lambda, \mu) & (\lambda_R, \mu_R) & (\lambda', \mu') & \tilde{\rho} \\ 1 & 1 & 1 & \end{Bmatrix}. \tag{B9}$$

The triply reduced matrix elements can be calculated from that of the π-boson creation and annihilation operators. In the former case they are

$$\langle (n_\pi', 0)|\big|\big| D_R^{(1,0)} \big|\big|\big| (n_\pi, 0)\rangle = \langle (n_\pi', 0)|\big|\big| \pi^{\dagger(1,0)} \big|\big|\big| (n_\pi, 0)\rangle = \delta_{n_\pi', n_\pi+1}(n_\pi + 1)^{1/2}. \tag{B10}$$

This result follows from the fact that $D_R^{(1,0)}$ is nothing but a π-boson creation operator coupled trivially to the σ-boson annihilating operator. A similar formula can be obtained for $D_R^{(0,1)}$ as follows:

$$\langle (n_\pi', 0)|\big|\big| D_R^{(0,1)} \big|\big|\big| (n_\pi, 0)\rangle = \langle (n_\pi', 0)|\big|\big| \pi^{(0,1)} \big|\big|\big| (n_\pi, 0)\rangle = \delta_{n_\pi', n_\pi-1}(n_\pi)^{1/2}. \tag{B11}$$

3. Matrix elements for the magnetic dipole transitions

Similarly to the quadrupole momentum matrix elements, there are three independent operators $L_j^{(1)}$, $j = 1, 2, R$, while the matrix elements of the dependent operators $L_C^{(1)} = L_1^{(1)} + L_2^{(1)}$ and $L = L_C^{(1)} + L_R^{(1)}$ can also be calculated in a simplified form. Actually, since these operators are also (rank-1) generators of the appropriate $\mathrm{SU}_j(3)$ group, their matrix elements can be evaluated in analogy to Eqs. (B3) to (B6) with the following considerations:

(i) Everywhere the isoscalar factor $\langle (\lambda, \mu)KL, (1, 1)12||(\lambda', \mu')K'L'\rangle_{\tilde{\rho}}$ appears it must be replaced with $\langle (\lambda, \mu)KL, (1, 1)11||(\lambda', \mu')K'L'\rangle_{\tilde{\rho}}$.

(ii) According to the convention used by Escher and Draayer [26], $L_{i\,m_j}^{(1)} = \boldsymbol{C}_{i\,m_j}^{(1,1)1\,1}$, so there is no additional coefficient to be considered for these matrix transition operators.

[1] J. Cseh, Phys. Lett. B **281**, 173 (1992).
[2] J. Cseh and G. Lévai, Ann. Phys. (NY) **230**, 165 (1994).
[3] G. Lévai, J. Cseh, and W. Scheid, Phys. Rev. C **46**, 548 (1992).
[4] K. Varga and J. Cseh, Phys. Rev. C **48**, 602 (1993); Zs. Fülöp, G. Lévai, E. Somorjai, Á. Z. Kiss, J. Cseh, P. Tikkanen, and J. Keinonen, Nucl. Phys. A **604**, 286 (1996); G. Lévai and J. Cseh, Phys. Lett. B **381**, 1 (1996); G. Lévai, J. Cseh, and P. Van Isacker, Eur. Phys. J. A **12**, 305 (1996); L. H. de la Peña, P. O. Hess, G. Lévai, and A. Algora, J. Phys. G **27**, 2019 (2001); G. Lévai, J. Cseh, and P. Van Isacker, *ibid.* **34**, 1729 (2001); J. Cseh, G. Lévai, and W. Scheid, Phys. Rev. C **48**, 1724 (2007); J. Cseh, R. K. Gupta, and W. Scheid, Phys. Lett. B **299**, 205 (1993); J. Cseh, Phys. Rev. C **50**, 2240 (1993); J. Cseh, G. Lévai, A. Ventura, and L. Zuffi, *ibid.* **58**, 2144 (1994); J. Cseh, G. Lévai, P. O. Hess, and W. Scheid, Few-Body Syst. **29**, 61 (1998); **29**, 61 (2000).
[5] H. Yépez-Martínez, P. O. Hess, A. Algora, J. Cseh, J. Darai, and G. Lévai, Rom. Rep. Phys. **59**, 717 (2007); J. Darai, J. Cseh, and P. O. Hess, AIP Conf. Proc. **1377**, 344 (2011).
[6] H. Yépez-Martínez, P. R. Fraser, and P. O. Hess, Rom. J. Phys. **57**, 513 (2012).
[7] G. Lévai and J. Cseh, Phys. Lett. B **381**, 1 (1996).
[8] P. O. Hess, G. Lévai, and J. Cseh, Phys. Rev. C **54**, 2345 (1996).
[9] T. A. Weaver and S. E. Woosley, Phys. Rep. **227**, 65 (1993).
[10] M. Hashimoto, Prog. Theor. Phys. **94**, 663 (1995).
[11] R. Plaga *et al.*, Nucl. Phys. A **465**, 291 (1987).
[12] J.-M. Sparenberg and P. Capel, and D. Baye, Phys. Rev. C **81**, 011601(R) (2010).
[13] R. G. Newton, *Scattering Theory of Waves and Particles*, 2nd ed. (Springer, New York, 1982).
[14] B. Buck and C. B. Dover, and J. P. Vary, Phys. Rev. C **11**, 1803 (1975).
[15] B. Buck and J. A. Rubio, J. Phys. G **10**, L209 (1984).
[16] M. Katsuma, Phys. Rev. C **78**, 034606 (2008).
[17] H. Makii, Y. Nagai, T. Shima, M. Segawa, K. Mishima, H. Ueda, M. Igashira, and T. Ohsaki, Phys. Rev. C **80**, 065802 (2009).
[18] K. Amos *et al.*, Nucl. Phys. A **728**, 65 (2003).
[19] L. Canton and L. G. Levchuk, Nucl. Phys. A **808**, 192 (2008).
[20] K. Wildermuth and Y. C. Tang, *A Unified Theory of the Nucleus* (Friedr. Vieweg & Sohn Verlagsgesselschaft mbH, Braunschweig, 1977).
[21] H. Yépez-Martínez, P. R. Fraser, P. O. Hess, and G. Lévai, Phys. Rev. C **85**, 014316 (2012).
[22] P. R. Fraser, H. Yépez-Martínez, P. O. Hess, and G. Lévai, Phys. Rev. C **85**, 014317 (2012).

[23] O. Castaños, P. O. Hess, P. Rochford, and J. P. Draayer, Nucl. Phys. A **524**, 469 (1991).
[24] J. Blomqvist and A. Molinari, Nucl. Phys. A **106**, 545 (1968).
[25] J. M. Eisenberg and W. Greiner, *Nuclear Theory I: Nuclear Models* (North-Holland, Amsterdam, 1987).
[26] J. Escher and J. P. Draayer, J. Math. Phys. **39**, 5123 (1998).
[27] D. J. Rowe and C. Bahri, J. Math. Phys. **41**, 6544 (2000).
[28] C. Bahri, D. J. Rowe, and J. P. Draayer, Comput. Phys. Commun. **159**, 121 (2004).
[29] O. Castaños, J. P. Draayer, and Y. Leschber, Z. Phys. A **329**, 33 (1988).
[30] J. Cseh, G. Lévai, P. O. Hess, and W. Scheid, Few-Body Systems **29**, 61 (2000).
[31] P. O. Hess, A. Algora, J. Cseh, and J. P. Draayer, Phys. Rev. C **70**, 051303 (2004).
[32] J. Cseh, G. Lévai, and K. Kato, Phys. Rev. C **43**, 165 (1991).
[33] K. Kato and H. Bando, Prog. Theor. Phys. **59**, 774 (1978).
[34] D. J. Rowe, Rep. Prog. Phys. **48**, 1419 (1985).
[35] http://www.nndc.bnl.gov/nndc/ensdf.
[36] M. Yasue *et al*., Phys. Rev. C **46**, 1242 (1992).
[37] R. M. Sellers *et al*., Bull. Am. Phys. Soc. **35**, 927 (1990).
[38] F. Ajzenberg-Selove, Nucl. Phys. A **460**, 70 (1986); **475**, 1 (1987).
[39] H. T. Richards, Phys. Rev. C **29**, 276 (1984).
[40] I. Kubo, Nucl. Phys. A **187**, 205 (1987).
[41] F. Aisenber-Selov, Nucl. Phys. A **392**, 1 (1983).
[42] G. Lévai, J. Cseh, and P. van Isacker, Eur. Phys. J. A **12**, 305 (2001).
[43] G. Lévai, J. Cseh, and P. van Isacker, J. Phys. G **34**, 1729 (2007).